# Atmospheric circulation compounds anthropogenic warming and impacts of climate extremes in Europe

Davide Faranda, Gabriele Messori, Aglaé Jézéquel, Mathieu Vrac, Pascal Yiou

▶ **To cite this version:**

Davide Faranda, Gabriele Messori, Aglaé Jézéquel, Mathieu Vrac, Pascal Yiou. Atmospheric circulation compounds anthropogenic warming and impacts of climate extremes in Europe. Proceedings of the National Academy of Sciences of the United States of America, 2023, 120 (13), pp.e2214525120. 10.1073/pnas.2214525120 . hal-03456537v3

**HAL Id: hal-03456537**
**https://hal.science/hal-03456537v3**

Submitted on 21 Mar 2023

**HAL** is a multi-disciplinary open access archive for the deposit and dissemination of scientific research documents, whether they are published or not. The documents may come from teaching and research institutions in France or abroad, or from public or private research centers.

L'archive ouverte pluridisciplinaire **HAL**, est destinée au dépôt et à la diffusion de documents scientifiques de niveau recherche, publiés ou non, émanant des établissements d'enseignement et de recherche français ou étrangers, des laboratoires publics ou privés.

# Atmospheric circulation compounds anthropogenic warming and impacts of climate extremes in Europe

**Davide Faranda**[a,b,c], **Gabriele Messori**[d,e], **Aglae Jezequel**[c,f], **Mathieu Vrac**[a], **and Pascal Yiou**[a]

[a]Laboratoire des Sciences du Climat et de l'Environnement, CEA Saclay l'Orme des Merisiers, UMR 8212 CEA-CNRS-UVSQ, Université Paris-Saclay & IPSL, 91191, Gif-sur-Yvette, France; [b]London Mathematical Laboratory, 8 Margravine Gardens, London, W6 8RH, UK; [c]Laboratoire de Météorologie Dynamique/IPSL, École Normale Supérieure, PSL Research University, Sorbonne Université, École Polytechnique, IP Paris, CNRS, Paris, 75005,France; [d]Department of Earth Sciences and Centre of Natural Hazards and Disaster Science (CNDS), Uppsala University, Uppsala, 752 36, Sweden; [e]Department of Meteorology and Bolin Centre for Climate Research, Stockholm University, 106 91, Stockholm, Sweden; [f]Ecole des Ponts, Marne-la-Vallée, France

This manuscript was compiled on January 16, 2023

**Diagnosing dynamical changes in the climate system, such as those in atmospheric circulation patterns, remains challenging. Here, we study 1950–2021 trends in the frequency of occurrence of atmospheric circulation patterns over the North Atlantic. Roughly 7% of atmospheric circulation patterns display significant occurrence trends, yet they have major impacts on surface climate. Increasingly frequent patterns drive heatwaves across Europe, and enhanced wintertime storminess in the northern part of the continent. Over 91% of recent heatwave-related deaths and 33% of high-impact windstorms in Europe were concurrent with increasingly frequent atmospheric circulation patterns. While the trends identified are statistically significant at the p-0.05 level, they are not necessarily anthropogenic. Atmospheric patterns which are becoming rarer correspond instead to wet, cool summer conditions over northern Europe and wet winter conditions over continental Europe. The combined effect of these circulation changes is that of a strong, dynamically-driven year-round warming over most of the continent and large regional and seasonal changes in precipitation and surface wind.**

Climate Change | Atmospheric Dynamics | European Windstorms | European Heatwaves

Extreme weather events exact a heavy and steadily increasing socio-economic toll on Europe(1), eliciting both scientific and media interest in the atmospheric circulation patterns favouring the occurrence of heatwaves(2), cold spells(3), heavy precipitation (4) and windstorms (5, 6). Such circulation patterns may be understood as spatial patterns in a given atmospheric variable which repeatedly occur in conjunction with specific classes of extreme events. The question of whether, how and why these circulation patterns have been changing under anthropogenic forcing, including the role of Arctic Amplification, has been the source of a lively discussion (7–25).

Of particular interest is whether atmospheric circulation patterns favouring specific extreme events have become more persistent. There are arguments supporting an increasingly persistent summer atmospheric circulation (10, 16, 18), which is highly relevant for the occurrence of heatwaves (19, 20). Nonetheless, (23) did not find a systematic slowdown of planetary waves over the Northern Hemisphere summers in the historical period, and (26) found no significant changes in their amplitude. There are also studies arguing against any projected changes in summertime atmospheric persistence, albeit on a regional scale (27). No consensus has therefore been reached on the topic. The picture for the winter season is equally debated, with some studies finding recent increases in the sinuosity of the midlatitude flow (11) and others not finding any trends in planetary wave phase speeds (23) or amplitude (26), or arguing for a decrease in high-amplitude waves and blocking — both regarded as persistent atmospheric patterns associated with surface extremes (8). A complementary line of work has analysed the frequency of occurrence of specific atmospheric circulation patterns associated with extreme events (9, 13–15, 24). Heatwaves have again been a focus, on account of their intimate link with the large-scale atmospheric circulation and rapidly increasing frequency and duration (25). For example, (9) found that well over half of the total trend in hot extremes over Europe may be linked to the increased occurrence of anticyclonic circulation patterns over the eastern part of the continent. Similarly, (15) argues that circulation patterns like the ones associated with the 2003 European heatwave may become increasingly frequent. Along a similar line, (24) identified observed changes in hemispheric-scale, wavy atmospheric circulation patterns that increase the risk of concurrent heatwaves across eastern North America, eastern and northern Europe and other downstream regions in Eurasia. Specific atmospheric patterns associated with other extremes, including drought (7) and heavy precipitation (21) have also been studied. The two perspectives of persistence and frequency of occurrence are intimately related, since re-

## Significance Statement

We address the key question of whether and how the dynamics of the atmosphere may enhance the impacts of anthropogenic climate change. We specifically focus on temperature and surface wind extremes in Europe, two classes of events which have caused a high death toll and large insured losses over the continent in the recent decades. We find that large scale atmospheric patterns which favor summertime heatwaves and wintertime windstorms over large parts of the continent are becoming increasingly frequent. This effect sums to that of the average global climate change. A key implication of our work is that circulation changes modulate extreme events already in the present climate.

D.F. conceived the study, performed the bulk of the analysis and compiled the European windstorm database. G.M performed the analysis on the EM-DAT database and contributed to compiling the European windstorm database. D.F and G.M, wrote and revised the manuscript. D.F., G.M., A.J., M.V. and P.Y. read and integrated the manuscript. .

The authors report no conflict of interest.

[2]To whom correspondence should be addressed. E-mail: davide.faranda@cea.fr

DRAFT

currence of a specific pattern likely translates to persistent weather and vice-versa (20).

Previous efforts in the detection of atmospheric circulation shifts have often focused on the average behaviour (11, 16, 23), for example presenting hemispheric or seasonal-mean results, or on a specific set of extreme events or reference circulation patterns (9, 15, 19, 24, 28, 29), for example the canonical North Atlantic weather regimes. Here, we consider in turn each daily atmospheric circulation pattern in 72 years of sea-level pressure reanalysis data (30), over the period 1950–2021 and the Euro-Atlantic sector. This results in 26280 daily sea-level pressure latitude-longitude maps. The same analysis is repeated using 500 hPa geopotential height data (See Supplementary Information). Our approach is thus distinct from the above-cited studies since we look at individual atmospheric circulation patterns without needing to select a priori a set of reference patterns. We then select those days in the winter (December–February) and summer (June–August) seasons displaying significant trends in the occurrence of their analogues (hereafter referred to simply as "occurrence trends" see Methods and Supplementary Information Figs. S1, S2). The vast majority (92.7%) of circulation patterns show no significant occurrence trend in the historical period; 5.1 % show increasing trends and 2.2 % show decreasing trends. Notwithstanding their rarity, the circulation patterns with significant occurrence trends have major implications for surface climate. To isolate the effect of circulation changes we also consider daily reanalysis data for 10 meter horizontal winds, 2 meter temperatures, and precipitation rates, over the same time-period and region. All the data shown in the composites are detrended and deseasonalized (see Methods).

During both the boreal summer and winter seasons, the atmospheric circulation patterns with positive occurrence trends show highly coherent surface climate anomalies over Europe. Specifically, patterns occurring more frequently in winter (Fig. 1a) show a north-south cyclonic-anticyclonic dipole. This is associated with anomalously windy, warm and wet conditions in Northern and Eastern Europe and moderately warm, dry conditions in Southern Europe (Fig. 1c, e, g). Wintertime patterns with a negative occurrence trend (Fig. 1b) have a cyclonic structure in the central North Atlantic and an anticyclone to the Northeast, leading to anomalously windy, cool and dry conditions over Northern Europe and windy, wet and moderately warm conditions over Central and Southern Europe (Fig. 1d, f, h). We next analyse the average wintertime temperature and precipitation associated with patterns displaying either decreasing or increasing occurrence trends over Europe (Fig. 1i, j; see mask in Supplementary Information Fig. S3). We do not detect additional significant circulation-related trends, besides the thermodynamics ones that have been already removed from the datasets (see methods). However, for 2 meter temperatures associated to patterns with increasing occurrence trends, the average value of 1.8–1.9 °C (black solid line, Fig 1i) is coherent with the large areas displaying positive 2 meter temperature anomalies in Fig. 1e).

In summer, the atmospheric circulation patterns with positive occurrence trends are associated with an anticyclonic anomaly over the Labrador Sea and Greenland and a cyclonic anomaly to the East of the British Isles (Fig. 2a). Such circulation patterns drive anomalously calm and dry conditions over much of the continent and anomalously warm conditions over Western Europe (Fig. 2c, e, g). Circulation patterns with decreasing occurrence trends show a ridge of high pressure anomalies over the Atlantic and a large cyclonic structure centred over Northern Europe. These are associated with anomalously calm conditions over most of Europe and cool and wet conditions over Northern Europe (Fig. 2d, f, h). Again, no significant trends appear in summertime European precipitation or temperature associated with any of the above patterns (Figs. 2i, j).

We underline that these results are obtained for detrended and deseasonalised datasets, meaning that the observed signals are chiefly related to the atmospheric circulation. Analyses conducted on NCEP/NCAR reanalysis data (Supplementary Information Figs. S4, S5) and E-OBS gridded observational data (Supplementary Information Figs. S6, S7) provide similar conclusions. Supplementary Information Figs. S8–S11 further show that the atmospheric circulation patterns with positive or negative occurrence trends are generally similar at the beginning and end of the analysis period. In other words, the atmospheric circulation patterns identified as having significant occurrence trends stay roughly constant over time. We further find that the identified trends are robust to changes in the details of our trend calculation (Supplementary Information Figs. S12-S17)

We repeat the same analysis for the detrended 500 hPa geopotential height data (Supplementary Information Figs. S18, S19), to verify whether our results depend on the choice of observable for the atmospheric circulation. There is a strong resemblance of the spatial anomaly composites for atmospheric circulation patterns with increasing frequency of occurrence in sea-level pressure and 500 hPa geopotential height, as well as the associated impacts on temperature, winds and precipitation (cf. Figs 1a, c, e, g, 2a, c, e, g and Supplementary Information Figs. S18a, c, e, g, and S19a, c, e, g). Patterns with decreasing frequency of occurrence show larger differences in both seasons (cf. Figs 1b, d, f, h, 2b, d, f, h and Supplementary Information Figs. S18b, d, f, h and S19b, d, f, h). This may be partly attributable to the smaller sample size for patterns with decreasing occurrence trends compared to patterns with increasing occurrence trends (approximately 43% of the sample size, computed jointly over winter and summer). It further suggests that our results for these sets of days should be interpreted with care. We conclude that the qualitative large-scale circulation patterns for days showing increasing occurrence trends and the associated surface anomalies are robust to the choice of the observable, while some notable differences emerge for days with decreasing occurrence trends. We estimate the magnitude of the trends for days showing significant positive or negative trends as number of analoges/decade for the different datasets and variables we consider here (see Table S1). Overall, we find that increasing (resp. decreasing) trends induce between 2 and 4 analogue occurrences more (resp. less) every decade.

The surface climate anomalies associated with increasingly or decreasingly frequent circulation patterns can be directly related to the occurrence of high-impact summertime heatwaves and wintertime stormy weather in Europe. We draw high-impact heatwaves and the associated excess deaths from the EM-DAT disaster database (31) (see Methods). We examine 228 heatwave days over the analysis period. 9.7% of these days correspond to atmospheric circulation patterns increasing

DRAFT

in occurrence (versus a climatological summertime occurrence of these patterns of 4.5% and a 97.5th percentile from random sampling of 7.0%), while none correspond to decreasing occurrence trends. As a term of comparison, only 3.1% of 480 cold spell days match atmospheric circulation patterns increasing in occurrence, in line with climatology. The 228 heatwave days occur during 10 major heatwave episodes, associated with 83,462 deaths. Four of these heatwaves include an above-average fraction of days with positive occurrence trends (see Methods). The latter heatwaves are responsible for 91.4% of the total heatwave-related excess deaths (Fig. 3a). Excluding from the analysis the summer 2003 heatwave, which is associated with days with positive occurrence trends and alone accounts for the bulk of the total heat-related deaths in Europe in the period considered, we still find that heatwaves associated with circulation patterns with positive occurrence trends are responsible for 43.2% of total excess deaths. Although this heuristic argument is based on a limited sample of events, it nonetheless serves to illustrate the potential societal impact that circulation patterns with increasing occurrence trends may have, and motivates a future, more systematic impact-based analysis.

We conduct a similar analysis for 90 European windstorms which resulted in a high number of casualties and/or large insured losses, extending the storm database from (32) (see Methods and Supplementary Information Fig. S20). Over a total of 438 windstorm days, we find that 66 (15%) are associated with circulation patterns with increasing occurrence trends and only 4 (0.9%) with patterns with decreasing trends. We find that 30 windstorms (33%) show an above-average fraction of days with positive occurrence trends while 4 events (4.4%) are linked to negative trends (Fig. 3b and Supplementary Information Fig. S20b). These statistics aggregate values on a continental level. A geographically-resolved picture highlights that the proportion of windstorms associated with patterns showing positive occurrence trends is larger in Continental/Northern Europe than in Southern Europe (Fig. 3b, e.g 40% in United Kingdom versus 0% in Italy). This is consistent with the pattern shown in Fig. 1c,g), which is reminiscent of the anomalies associated with destructive windstorms over Continental Europe found by (5).

In this paper, we identified the atmospheric circulation patterns over the North Atlantic and Europe that have become less or more frequent in the historical period. We based our analysis on all daily patterns in the data, rather than on aggregated patterns, average behaviour or a specific set of extreme events or reference circulation patterns (9, 11, 15, 16, 19, 23, 24, 28, 29). In other words, we do not constraint our analysis to a fixed number of reference spatial patterns of some atmospheric field, but rather view each atmospheric pattern as unique and characterised by rare recurrences (a few % of all data in our analysis). This approach does not require introducing any specific decomposition bases and the associated hyperparameters. We are thus able to isolate robust linear trends in the frequency of occurrence of specific, observed circulation patterns. Our results show minimal differences if a quadratic or cubic fit is applied instead of a linear one. The difference from previous studies is not only methodological, but also interpretative. For example, we find increasing occurrence of zonal flow patterns and decreasing occurrence of antizonal patterns over the North Atlantic during winter, which do not emerge from a conventional weather regime-based perspective (33, 34).

Our method is flexible, and could for example be used as a complement to extreme event attribution studies conditioned on the circulation (35, 36), akin to the storyline approach (37). The latter approach has been criticized for not taking into account the role of climate change-induced circulation changes (38), and we provide a readily applicable toolkit to address this problem. Our approach is not data or location-specific, and may be applied to different regions or datasets. This makes it well-suited as a tool to evaluate the consistency of dynamical trends in numerical simulations with those observed in reanalysis data. In the future, our approach could be complemented by the use of machine learning techniques for identifying atmospheric analogues, as opposed to using the Euclidean distance (e.g. 39).

Our analysis does not enable to make a robust statement as to the potential role of natural variability versus anthropogenically-driven climate change in modulating the trends in atmospheric circulation pattern occurrence over the recent decades. An analysis of climate modes of low-frequency variability highlights a possible modulation of the El Niño–Southern Oscillation and the North Atlantic Oscillation variability on trends in circulation pattern occurrence (see Supplementary Information and Supplementary Information Figs. S21–S23), which should be taken into consideration when interpreting our results. Indeed, recent work has suggested that the variability of the North Atlantic Oscillation can modulate decadal temperature trends (33). In future work, one may also leverage initial condition large ensembles to separate forced signals from internal variability in the context of our analogue analysis (e.g. 40). A further limitation of our study is that it assumes that the circulation patterns of interest have good analogues in the dataset being used (see Methods). This assumption is problematic in the presence of strong non-stationarities, which may lead to unprecedented atmospheric states. A theoretical advance would be to complement the analysis with a systematic investigation of analogue quality, based on the distance between a day and its analogues. Preliminary analyses to this effect show no long-term trends in analogue quality, yet highlight some interannual variability which may relate to the above-discussed El Niño–Southern Oscillation modulation. A second caveat is that the analysis of surface impacts through the EM-DAT and the windstorms database likely suffers from temporal and spatial inconsistencies in reporting — a common limitation of impacts data (41). In our specific case, the partial reliance of the windstorms database on catalogues compiled for the scientific literature (see Methods), could alleviate the issue, but by no means completely resolves it.

We underscore that the temperature anomalies associated with increasingly frequent circulation patterns (Figs. 1e, 2e) are regionally comparable to or larger than the average global climate change (+1.07°C, best estimates reported the IPCC(42)) with winter (summer) temperatures anomalies up to +5.7°C (+1.1°C). These results are obtained after detrending and deseasonalising the data, and are consistent with those obtained for the 500 hPa geopotential height in the Supplementary Information.

The circulation types we study, while rare (approximately 7% of all winter and summer days in our dataset), are in-

DRAFT

creasing and decreasing at a pace of about 2-4 analogues per decade, depending on the variable and dataset examined (see Table S1). If these trends are due to anthropogenic forcing, we expect the circulation patterns with positive occurrence trends to dominate the respective seasons in 2–4 decades. If, instead, they are due to internal variability, we expect to continue seeing their footprint for the next few decades. Regardless of their origin, we stress that these circulation patterns are associated with impactful extreme events, both deadly heatwaves and destructive windstorms. While these events are not exclusively caused by circulations changes, our results show that circulation changes cannot be neglected when evaluating the consequences of anthropogenic climate change or other sources of climatic variability on extreme weather events and their impacts.

## Materials and Methods

**Computing trends in the occurrence of atmospheric circulation patterns.** For the computation of the trends in the occurrence of atmospheric circulation pattern analogues (which we hereafter refer to as "occurrence trends"), we use daily sea level pressure and 500hPa geopotential height data from the ERA5 reanalysis (30) over the period 01/01/1950 – 31/12/2021 (26,280 days). This is the sample size for all analyses presented in the manuscript. The data have a horizontal resolution of $0.25° \times 0.25°$, and we restrict our analysis to 22.5N – 70N and 80W – 50E. This corresponds to the North Atlantic and Europe, with a size of $200 \times 530$ grid cells. Part of the analysis was repeated on additional datasets and subperiods of the full dataset (see Supplementary Information). For both the sea-level pressure and 500 hPa geopotential height data, we remove a grid point by grid point linear trend for the whole analysis period. This ensures that the selection of circulation analogues is not affected by long-term thermodynamic trends. We further deseasonalise the data using a mean seasonal cycle computed by averaging over the same calendar days. The robust trends in the occurrence of atmospheric circulation patterns are computed as follows:

1. We select daily sea-level pressure or 500 hPa geopotential height latitude–longitude maps, which we interpret as atmospheric circulation patterns.
2. We compute the Euclidean distance between daily maps, taking each daily map in turn as reference state and computing its distance from all other maps in the dataset. We then define a high quantile $q$ to select the analogues. We chose $q = 0.98$, meaning that we take as analogues the 2% closest fields to the target. We describe below how the sensitivity to the choice of $q$ is tested.
3. We divide the time interval of 73 years into 9 periods of roughly 8 years. We then count how many analogues $N$ fall in each period $t$, obtaining $N(t)$ with $0 < t \leq 9$. Shortening these periods has no qualitative impact on our results (see Supplementary Figs. S12, S13).
4. We perform a linear fit of $N(t)$ of the type $at+b$. Using a cubic fit does not qualitatively affect the results (Figs. S14-S15).
5. We estimate the upper and lower 95% confidence intervals (CI) of the $a$ parameter of the fit using the Wald method (43). If the lower and the upper bounds of the CI for $a$ are positive (negative), we interpret this as a significant positive (negative) trend for the selected daily sea-level pressure or 500 hPa geopotential height map and quantile $q$. If the confidence interval contains zero, the trend is non-significant.
6. We repeat the above steps for $q = 0.99$ and $q = 0.995$. We retain as daily maps with significant increasing (decreasing) occurrence trends only those having consistent (same sign AND significant) occurrence trends for all three quantiles. These are the robust circulation patterns that are analysed in this paper. We additionally verify that the quality (i.e. distance) of analogues for these patterns is comparable to that for all other days in our dataset.

The 95% CIs that we compute indicate that there is a 5% chance that the real trend is out of the CI interval. Since the CIs are defined as symmetrical intervals, this implies that the chance that the "real" trend is zero or of opposite sign to that of our sample is $\leq 2.5\%$. In practice, since we use three different quantiles $q$ simultaneously, this chance is very small, even taking into account that these are not independent samples. While analogues are a relatively common analysis approach in the atmospheric sciences, our methodology and its focus on trends is novel. It is further fundamentally different from conventional decompositions of the atmospheric variability, such as self-organsing maps (44), k-means clustering (45), Empirical Orthogonal Functions or others (46). Indeed, we do not constraint our analysis to a fixed number of circulation patterns. The occurrence trends are thus identified for daily patterns rather than for a fixed pattern associated with, e.g. a self-organising map or weather regime. Indeed, the computation of the analogues does not require introducing any specific decomposition bases, which in turn introduce arbitrary hyperparameters such as the number of components into which the atmospheric variability is partitioned. Moreover, we do not "create" reference fields that may have never been observed in the data by orthogonal decomposition, averaging or centroid computations. Our approach thus relies directly on the atmospheric variability present in the data, without adding an intermediate projection step.

**Computation of Significant Circulation and Surface Anomalies.** After identifying the circulation patterns with robust increasing or decreasing occurrence trends for the whole year, we produce composite anomalies for the patterns on days within the winter (DJF) and summer (JJA) months (without including their analogues) for several daily variables: sea-level pressure, 500 hPa geopotential height, horizontal 10m wind speed and precipitation rate. All these data are detrended and deseasonalised using the same procedure as for sea-level pressure and 500 hPa geopotential height. Significance for the geographical anomalies is estimated by using a bootstrap procedure (sample size $m = 500$) consisting in randomly drawing from the whole dataset a number of days equal to the number of days in each composite, regardless of their trend. Significant anomalies are those below the 5th or above the 95th percentiles of the bootstrap distribution at each grid point. We have also tested gridpoint by gridpoint sign agreement of the days within each composite, to ensure that the composite anomalies result from a spatially coherent set of daily anomalies (S16-S17). Long term trends shown in the composites of Figs. 1–2 and Supplementary Information Figs. S4–S19 are computed by averaging, for each season, the spatial averages over Europe (see mask in Supplementary Information Fig. S3) for the patterns displaying occurrence trends. Years without patterns displaying occurrence trends are treated as NaNs. Significance for trends is estimated by using the Wald method and looking at the sign of both the upper and lower bounds of the CI. CIs of trends are displayed in the legends of the relevant figure panels.

**Computing impacts of atmospheric circulation patterns with positive occurrence trends.** We take heat waves and cold spells from the EM-DAT disaster database (31). We focus on events over Western-Central Europe (excluding e.g. Western Russia, outlying islands such as the Canary Islands etc.), excluding those heat waves and cold spells where no start and/or end day was provided, or which lasted only for one day. Dates included in several events were only counted once. Following these criteria, from a total of 34 heatwave and 66 cold spell episodes included in EM-DAT, we identified 228 days over 10 heatwaves and 480 days over 16 cold spells. Of the original 34 heatwave events, 3 were excluded because they were entirely outside Europe, 11 because they were missing start and/or end dates, 9 because a single day was assigned to the heatwave. Finally 2 heatwaves were merged into 1 because, even though they had different “disaster numbers” (i.e. unique identifiers of each disaster in EM-DAT), they had overlapping dates and occurred in geographically contiguous regions. Of the 66 cold spells, a relatively large number was excluded due to being outside of Europe (13 events were only registered in Russia). An additional 35 were excluded due to missing or single-day dates. Finally, four events were merged into 2 because, even though they had different “disaster numbers”, they had overlapping dates and occurred in geographically contiguous

DRAFT

regions.

European Windstorms data is taken from an updated version of the storm database of (32), which originally covered the period 1948–2015. This database is largely based on the catalogues by (47) (ending 1972) and (48) (ending 2014). Additional windstorms (2015–2020) have been integrated from the Wikipedia web-page https://en.wikipedia.org/wiki/List_of_European_windstorms because of their relevance in terms of human losses, damages or their profile in the media. We have only selected windstorms that have been analyzed by a meteorological office or research institute: a link to the documentation is provided together with each entry in the database. The database itself is available as Supplementary Data. Using publicly contributed databases as sources for scientific information is becoming a common practice in citizen science projects, which are gaining momentum in the geosciences (49, 50). Our database includes a total of 438 windstorm days and 90 distinct windstorms or windstorm clusters. Supplementary Information Fig. S20 presents the database entries per country (a) and per time of occurrence (b).

The database is organized in four columns:

1. The day of occurrence in the format yyyymmdd;
2. The name(s) of the windstorm;
3. The country/countries or the region(s) affected;
4. A reference to a peer-reviewed article, a report or a press article describing the importance of the windstorm.

As a caveat to our methodology, we note that the increasing coverage of both meteorological instruments and technological means of information result in an increasing number of windstorms with time.

To determine whether a given extreme event is associated to circulation patterns with positive or negative occurrence trends, we first compute the fraction of days with positive occurrence trends within each extreme event. We then compare these fractions to the average frequency of occurrence of circulation patterns with positive or negative occurrence trends within the 20 years centered on the extreme. This is because the frequency of occurrence of atmospheric circulation patterns with positive occurrence trends is by definition higher in the later part of the data than in the earlier years, such that each extreme should be compared to the period within which it occurs. Based on this comparison, we then separate extreme events into groups which have an above or below-average fraction of daily analogues with either trend.

**ACKNOWLEDGMENTS.** D.Faranda, M. Vrac, P. Yiou received funding under the European Union's Horizon 2020 research and innovation programme (Grant agreement No. 101003469, XAIDA). D. Faranda, G. Messori and P. Yiou received funding under the European Union's Horizon 2020 research and innovation programme (Marie Skłodowska-Curie Grant agreement No. 956396, EDIPI). G. Messori received funding from the European Research Council (ERC) under the European Union's Horizon 2020 research and innovation programme (Grant agreement No. 948309, CENÆ). D. Faranda acknowledges the support of the ANR-TERC grant BOREAS ANR-19-ERC7-0003 and the LEFE-MANU-INSU-CNRS grant DINCLIC. P. Yiou was supported by the French ANR (grant No. ANR-20-CE01-0008-01, SAMPRACE). All authors thank the anonymous reviewers and the editor for their support in improving the study.

1. Forzieri G, et al. (2018) Escalating impacts of climate extremes on critical infrastructures in europe. *Global environmental change* 48:97–107.
2. Sousa PM, et al. (2020) Distinct influences of large-scale circulation and regional feedbacks in two exceptional 2019 european heatwaves. *Communications Earth & Environment* 1(1):1–13.
3. Lehmann J, Coumou D (2015) The influence of mid-latitude storm tracks on hot, cold, dry and wet extremes. *Scientific reports* 5(1):1–9.
4. Zanardo S, Nicotina L, Hilberts AG, Jewson SP (2019) Modulation of economic losses from european floods by the north atlantic oscillation. *Geophysical Research Letters* 46(5):2563–2572.
5. Hanley J, Caballero R (2012) The role of large-scale atmospheric flow and rossby wave breaking in the evolution of extreme windstorms over europe. *Geophysical Research Letters* 39(21).
6. Messori G, Caballero R (2015) On double rossby wave breaking in the north atlantic. *Journal of Geophysical Research: Atmospheres* 120(21):11–129.
7. Vicente-Serrano SM, López-Moreno JI (2006) The influence of atmospheric circulation at different spatial scales on winter drought variability through a semi-arid climatic gradient in northeast spain. *International Journal of Climatology: A Journal of the Royal Meteorological Society* 26(11):1427–1453.
8. Hassanzadeh P, Kuang Z, Farrell BF (2014) Responses of midlatitude blocks and wave amplitude to changes in the meridional temperature gradient in an idealized dry gcm. *Geophysical Research Letters* 41(14):5223–5232.
9. Horton DE, et al. (2015) Contribution of changes in atmospheric circulation patterns to extreme temperature trends. *Nature* 522(7557):465–469.
10. Coumou D, Lehmann J, Beckmann J (2015) The weakening summer circulation in the northern hemisphere mid-latitudes. *Science* 348(6232):324–327.
11. Cattiaux J, Peings Y, Saint-Martin D, Trou-Kechout N, Vavrus SJ (2016) Sinuosity of midlatitude atmospheric flow in a warming world. *Geophysical Research Letters* 43(15):8259–8268.
12. Horton RM, Mankin JS, Lesk C, Coffel E, Raymond C (2016) A review of recent advances in research on extreme heat events. *Current Climate Change Reports* 2(4):242–259.
13. Mann ME, et al. (2017) Influence of anthropogenic climate change on planetary wave resonance and extreme weather events. *Scientific reports* 7(1):1–12.
14. Jézéquel A, Yiou P, Radanovics S, Vautard R (2017) Analysis of the exceptionally warm december 2015 in france using flow analogues. *Bulletin of the American Meteorological Society*.
15. Jézéquel A, et al. (2018) Trends of atmospheric circulation during singular hot days in europe. *Environmental Research Letters* 13(5):054007.
16. Coumou D, Di Capua G, Vavrus S, Wang L, Wang S (2018) The influence of arctic amplification on mid-latitude summer circulation. *Nature Communications* 9(1):1–12.
17. Mann ME, et al. (2018) Projected changes in persistent extreme summer weather events: The role of quasi-resonant amplification. *Science advances* 4(10):eaat3272.
18. Routson CC, et al. (2019) Mid-latitude net precipitation decreased with arctic warming during the holocene. *Nature* 568(7750):83–87.
19. Kornhuber K, et al. (2019) Extreme weather events in early summer 2018 connected by a recurrent hemispheric wave-7 pattern. *Environmental Research Letters* 14(5):054002.
20. Röthlisberger M, Frossard L, Bosart LF, Keyser D, Martius O (2019) Recurrent synoptic-scale rossby wave patterns and their effect on the persistence of cold and hot spells. *Journal of Climate* 32(11):3207–3226.
21. Barlow M, et al. (2019) North american extreme precipitation events and related large-scale meteorological patterns: a review of statistical methods, dynamics, modeling, and trends. *Climate Dynamics* 53(11):6835–6875.
22. Cohen J, et al. (2020) Divergent consensuses on arctic amplification influence on midlatitude severe winter weather. *Nature Climate Change* 10(1):20–29.
23. Riboldi J, Lott F, d'Andrea F, Rivière G (2020) On the linkage between rossby wave phase speed, atmospheric blocking, and arctic amplification. *Geophysical Research Letters* 47(19):e2020GL087796.
24. Rogers CD, Kornhuber K, Perkins-Kirkpatrick SE, Loikith PC, Singh D (2022) Sixfold increase in historical northern hemisphere concurrent large heatwaves driven by warming and changing atmospheric circulations. *Journal of Climate* 35(3):1063–1078.
25. Perkins-Kirkpatrick S, Lewis S (2020) Increasing trends in regional heatwaves. *Nature communications* 11(1):1–8.
26. Blackport R, Screen JA (2020) Insignificant effect of arctic amplification on the amplitude of midlatitude atmospheric waves. *Science advances* 6(8):eaay2880.
27. Huguenin MF, et al. (2020) Lack of change in the projected frequency and persistence of atmospheric circulation types over central europe. *Geophysical Research Letters* 47(9):e2019GL086132.
28. Corti S, Molteni F, Palmer T (1999) Signature of recent climate change in frequencies of natural atmospheric circulation regimes. *Nature* 398(6730):799–802.
29. Cassou C, Cattiaux J (2016) Disruption of the european climate seasonal clock in a warming world. *Nature Climate Change* 6(6):589–594.
30. Hersbach H, et al. (2015) Era-20cm: A twentieth-century atmospheric model ensemble. *Quarterly Journal of the Royal Meteorological Society* 141(691):2350–2375.
31. Guha-Sapir D (2017) Em-dat: The emergency events database–université catholique de louvain (ucl)–cred, brussels, belgium.
32. Faranda D, Messori G, Yiou P (2017) Dynamical proxies of north atlantic predictability and extremes. *Scientific reports* 7(1):1–10.
33. Iles C, Hegerl G (2017) Role of the north atlantic oscillation in decadal temperature trends. *Environmental Research Letters* 12(11):114010.
34. Matsueda M, Palmer T (2018) Estimates of flow-dependent predictability of wintertime euro-atlantic weather regimes in medium-range forecasts. *Quarterly Journal of the Royal Meteorological Society* 144(713):1012–1027.
35. Meredith EP, Semenov VA, Maraun D, Park W, Chernokulsky AV (2015) Crucial role of black sea warming in amplifying the 2012 krymsk precipitation extreme. *Nature Geoscience* 8(8):615–619.
36. Trenberth KE, Fasullo JT, Shepherd TG (2015) Attribution of climate extreme events. *Nature Climate Change* 5(8):725–730.
37. Shepherd TG (2016) A common framework for approaches to extreme event attribution. *Current Climate Change Reports* 2(1):28–38.
38. Otto FE, et al. (2016) The attribution question. *Nature Climate Change* 6(9):813–816.
39. Thomas C, Voulgarakis A, Lim G, Haigh J, Nowack P (2021) An unsupervised learning approach to identifying blocking events: the case of european summer. *Weather and Climate Dynamics* 2(3):581–608.
40. Deser C, et al. (2020) Insights from earth system model initial-condition large ensembles and future prospects. *Nature Climate Change* 10(4):277–286.
41. Gall M, Borden KA, Cutter SL (2009) When do losses count? six fallacies of natural hazards loss data. *Bulletin of the American Meteorological Society* 90(6):799–810.
42. IPCC (2021) *Summary for Policymakers*, eds. Masson-Delmotte, V. PZAPSCCPSBNCY-

DRAFT

CLGMGMHKLELJMTMTWOYRY, Zhou B. (Cambridge University Press, Cambridge, United Kingdom and New York, NY, USA), p. 1–42.
43. Stein C, Wald A (1947) Sequential confidence intervals for the mean of a normal distribution with known variance. *The Annals of Mathematical Statistics* pp. 427–433.
44. Kohonen T (1990) The self-organizing map. *Proceedings of the IEEE* 78(9):1464–1480.
45. Dunn OJ (1961) Multiple comparisons among means. *Journal of the American statistical association* 56(293):52–64.
46. Hannachi A, Straus DM, Franzke CL, Corti S, Woollings T (2017) Low-frequency nonlinearity and regime behavior in the northern hemisphere extratropical atmosphere. *Reviews of Geophysics* 55(1):199–234.
47. Lamb HH (1972) British isles weather types and a register of the daily sequence of circulation patterns 1861-1971.
48. Roberts J, et al. (2014) The xws open access catalogue of extreme european windstorms from 1979 to 2012. *Natural Hazards and Earth System Sciences* 14(9):2487–2501.
49. Fritz S, et al. (2012) Geo-wiki: An online platform for improving global land cover. *Environmental Modelling & Software* 31:110–123.
50. Sparrow S, et al. (2021) Openifs@ home version 1: a citizen science project for ensemble weather and climate forecasting. *Geoscientific Model Development* 14(6):3473–3486.

DRAFT

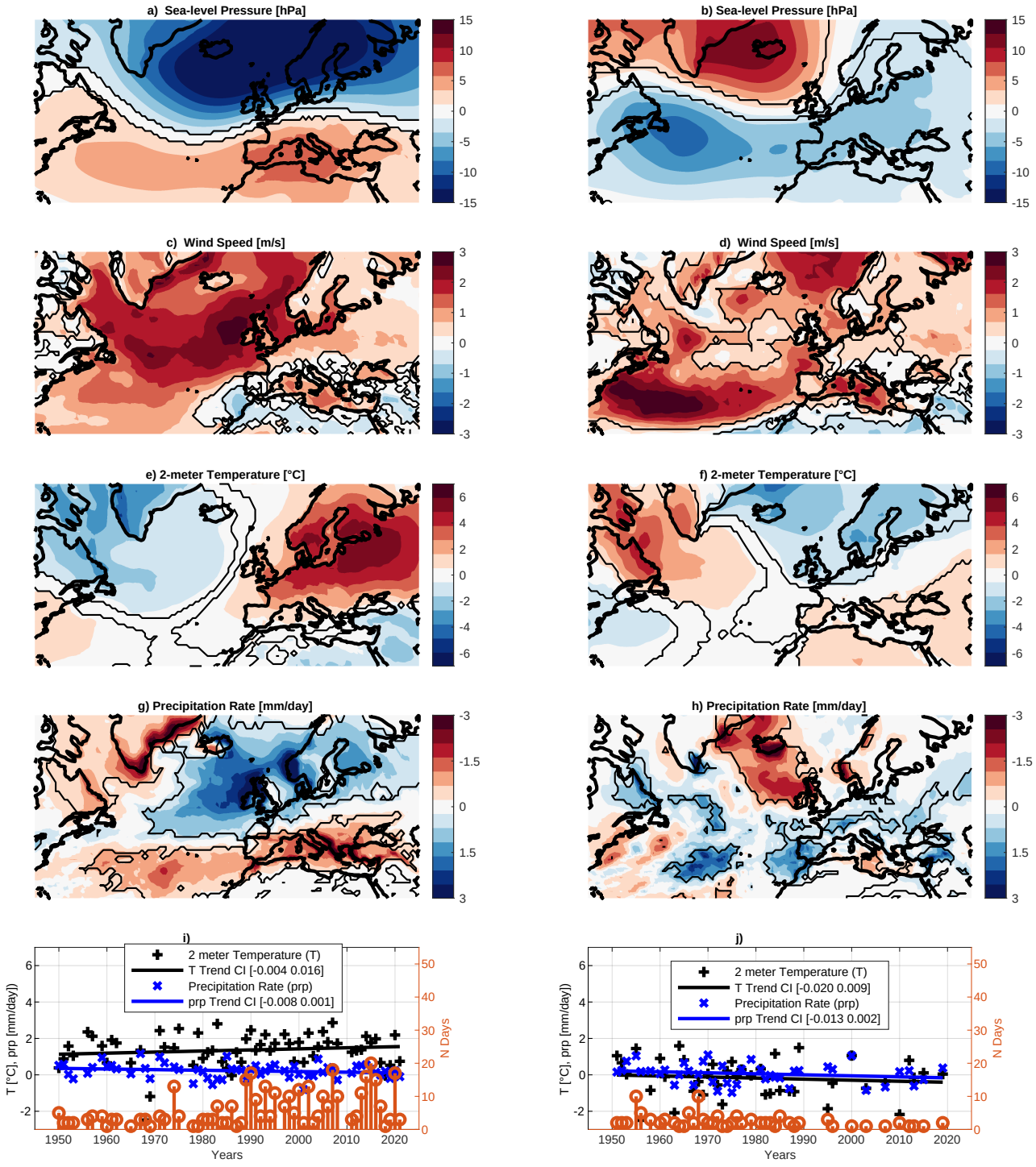


**Fig. 1. Sea-level pressure wintertime atmospheric circulation patterns with significant occurrence trends and associated surface anomalies:** Composite anomalies of DJF sea-level pressure (a,b), 10m horizontal wind speed (c,d), 2-meter temperatures (e,f) and precipitation rates (g,h) for days with increasing (a,c,e,g) or decreasing (b,d,f,h) occurrence trends. In the composites (a–h), contours indicate regions with changes significant at the onse-sided 5% level, computed with a bootstrap sample size of 500. Spatial averages of seasonal temperature anomalies (black) and precipitation rates (blue) during the days with increasing (i) or decreasing (j) occurrence trends and count of days displaying the corresponding occurrence trend (orange stems) during DJF. Solid lines represent linear trends of the spatial averages with the 95% confidence intervals of the two linear fits in each panel shown in the legends. The averages in (i), (j) are computed on all European land points (see Supplementary Information Fig. S3).

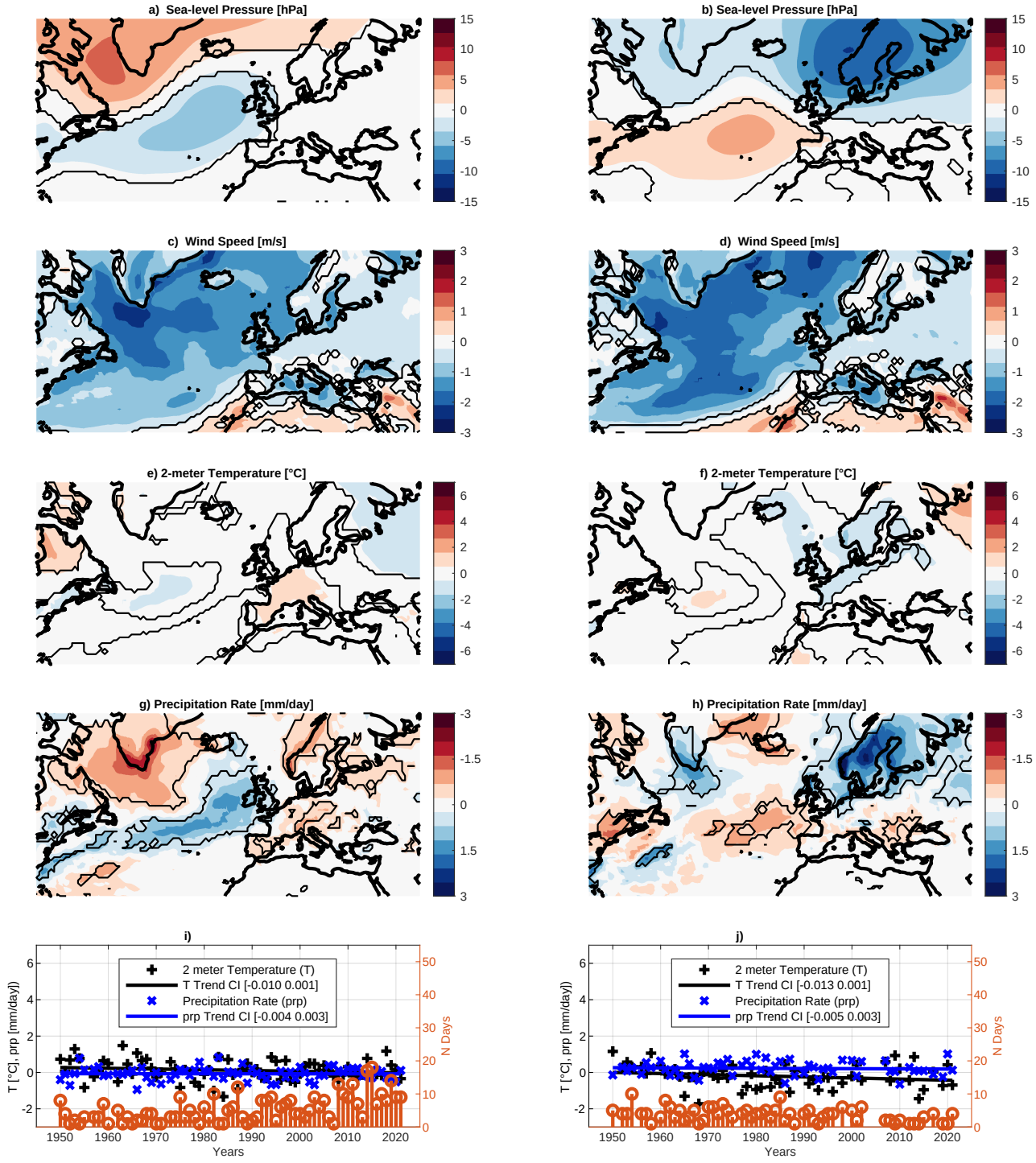


**Fig. 2. Sea-level pressure summertime atmospheric circulation patterns with significant occurrence trends and associated surface anomalies:** As in Fig. 1, but for JJA.

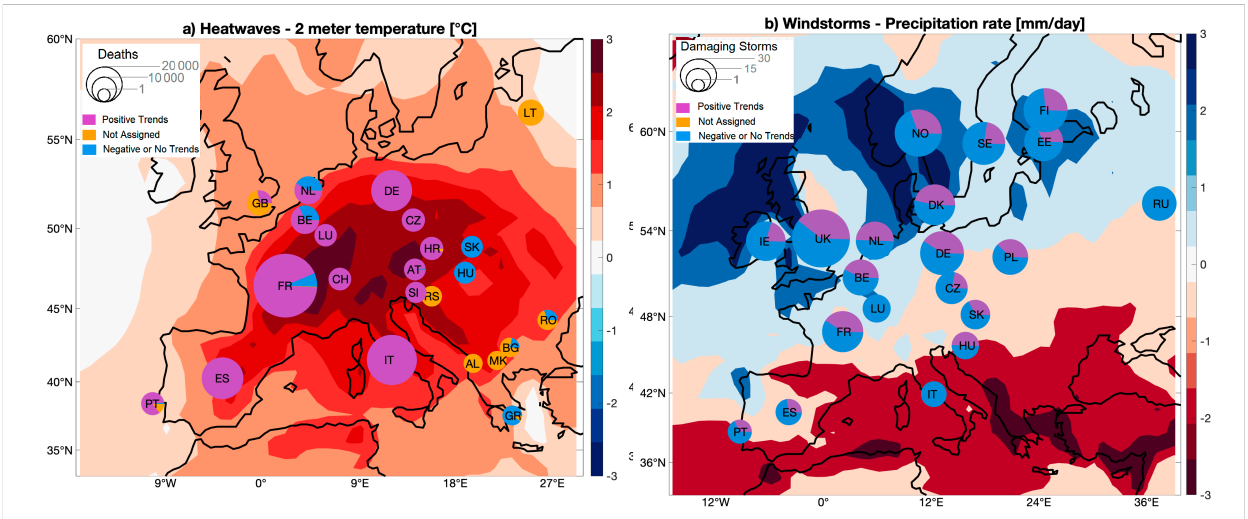


**Fig. 3. Impacts of changing atmospheric circulation patterns in terms of heatwave casualties and European Windstorms.** (a) The size of the pie chart for each country shows the total number of heatwave excess deaths as recorded in the EM-DAT database for the whole year. The purple slices show the fraction of excess deaths associated with heatwaves showing an above-average frequency of circulation patterns with a positive occurrence trend. The yellow slices show the excess deaths associated with heatwaves that we excluded from our analysis (see Methods). Finally, the blue slices show the corresponding fractions for heatwaves showing circulation patterns with no or negative occurrence trends. The shading on the geographical map shows the temperature anomalies (°C) during the 228 heatwave days retained for analysis. (b) The size of the pie chart for each country shows the total number of destructive windstorms in the storm database for the whole year (see Methods). The purple slices show the fraction of windstorms showing an above-average frequency of circulation patterns with a positive occurrence trend. The blue slices show the corresponding fraction for windstorms showing analogues with no or negative occurrence trends. The shading on the geographical map shows the precipitation anomalies (mm day$^{-1}$) during the 438 windstorm days retained for analysis.

# Supporting Information for

## Atmospheric circulation compounds anthropogenic warming and impacts of climate extremes in Europe

**Davide Faranda, Gabriele Messori, Aglae Jezequel, Mathieu Vrac, and Pascal Yiou**

**Corresponding Author: Davide Faranda.**
**E-mail: davide.faranda@cea.fr**

### This PDF file includes:

## Use of additional datasets

In addition to the ERA5 data used in the main text, we have repeated the computation of occurrence trends of atmospheric circulation patterns using sea-level pressure from the NCEP/NCAR reanalysis (1) (Figs. S4, S5) and 2m-temperature and precipitation from E-OBS v25.0e over land (Figs. S6, S7). We use both datasets over the same period as in the main analysis, namely 01/01/1950 – 31/12/2021. The NCEP/NCAR data has a horizontal resolution of $2.5^\circ \times 2.5^\circ$, while the E-OBS v25.0e data has a horizontal resolution of $0.25^\circ \times 0.25^\circ$. We restrict our analysis to the same 80W – 50E and 22.5N – 70N domain used in the main text. Figures S4, S6 and S5, S7 correspond respectively to Figs. 1 and 2 computed for ERA5. Allowing for the different spatial resolutions of the datasets, which result in some modulation of the intensity of the anomalies, the corresponding patterns in all variables and seasons closely resemble each other. The fact that very different datasets provide the same conclusions supports the robustness of our analysis.

## Analysis on sea-level pressure and 500 hPa geopotential height

We identify days with significant occurrence trends using analogues computed on either sea-level pressure or 500 hPa geopotential height. In winter, we note a very close resemblance of the 500 hPa geopotential height and sea-level pressure large-scale patterns for days with increasing occurrence trends. In both cases, the anomaly structure is an NAO-like meridional dipole favouring an intensified zonal flow. This leads to very similar surface anomalies (cf. Figs. 1a, c, e, g and S18a, c, e, g). For the wintertime decreasing occurrence trends, the 500 hPa geopotential height pattern has a marked meridional and quadripolar structure, while the sea-level pressure pattern is chiefly dipolar and anti-zonal. The surface anomalies over Europe are regionally different, although especially for precipitation some of the large-scale features are comparable (cf. Figs. 1b, d, f, h and S18b, d, f, h). A similar picture emerges for summer (Figs. 2 and S19). The large-scale patterns for days with increasing occurrence trends are broadly similar: both variables display a mid-Atlantic trough and a zonally extended band of positive anomalies in the northernmost part of the domain. We nonetheless note a meridional shift in the anomaly poles and the fact that 500 hPa geopotential height shows comparatively larger positive anomalies over Scandinavia. The patterns for decreasing occurrence trends again show larger differences. In the case of sea-level pressure, there is a dipolar pattern with the positive pole to the North of the Azores and the negative pole over Scandinavia. The 500 hPa geopotential height anomaly pattern is wave-like. This is to some extent also mirrored in the surface anomalies (cf. Figs. 2b, d, f, h and S19b, d, f, h). The scale would appear comparable to the wave-5 pattern of (2), although the surface temperature anomalies do not match those of the latter study. The pattern also resembles the Node 7 500 hPa geopotential height pattern shown in (3), although the latter study finds that this pattern has a significantly increasing occurrence trend over the historical period, contrary to what we find in our analysis. The regional North Atlantic view we take may explain part of the discrepancy with the circumhemispheric wave view of (2, 3).

## Modulation of circulation pattern occurrences by natural variability

The atmospheric circulation pattern occurrence trends we identified in our analysis may be modulated by natural variability. To investigate this, we have analysed the correspondence between atmospheric circulation pattern occurrence trends and the El Nino–Southern Oscillation (ENSO) as diagnosed through the Nino 3.4 index, the Atlantic Multidecadal Oscillation (AMO) and the North Atlantic Oscillation indices. Specifically, we have tested whether days with positive or negative occurrence trends correspond to anomalous ENSO, AMO or NAO values and whether high or low ENSO, AMO or NAO values favour positive or negative occurrence trends. For ENSO and AMO, we have conducted the analysis using monthly indices computed from the NOAA/ERSSTv5 dataset (4) and for NAO, we used the monthly NOAA Climate prediction center teleconnection index (5) retrieved from KNMI's climate explorer. The Nino 3.4 timeseries is normalised over the 1981–2010 period, while the AMO timeseries is normalised over the 1971–2010 period. For the NAO index, the standardized anomalies are calculated based on the 1950–2000 climatological daily mean and standard deviations. Thus none of these indices have a zero average over the analysis period we consider. The Nino 3.4 index has shown an upward trend in recent decades (6, 7), something which we also see in our data. The AMO and NAO indices also show a weak trend. We have therefore conducted our analysis on both the raw and linearly detrended timeseries (the latter being centred on zero due to the detrending process). There is a clear association between ENSO variability and atmospheric circulation pattern occurrence trends. Nino 3.4 values are significantly positive (negative) for days with positive (negative) occurrence trends (Fig. S21a,b). Similarly, days with positive (negative) occurrence trends show a clear preference for months in the upper (lower) tertiles of the Nino 3.4 distribution (Fig. S21c,d). The above holds for both the raw and detrended Nino 3.4 timeseries, although the results in Fig. S21c,d are stronger for the undetrended ENSO timeseries. We thus conclude that there appears to be a statistical modulation of ENSO variability on trends in the occurrence of atmospheric circulation patterns in the North Atlantic sector, and that the association between positive (negative) ENSO phases and days with positive (negative) occurrence trends is stronger if the long-term ENSO trend is taken into account. Focussing on days with positive occurrence trends, during winter we hypothesise that this may be linked to the NAO-like footprint of ENSO on North Atlantic sea-level pressure (8). During summer the picture is not as clear, and recent work has found only weak relations between ENSO and the summer NAO (9). For the NAO index itself, we only find a clear association with days with increasing occurrence trends (Fig. S22c), which tend to be associated with positive NAO phases. This is expected on the basis of the pattern obtained in Figure 1a as it consists of a strong zonal flow typically associated with positive phases of the North Atlantic Oscillation index. No significant association between atmospheric circulation pattern occurrence trends and the AMO has been instead detected (Fig. S23).

Notwithstanding the possible low-frequency modulation of the atmospheric circulation pattern occurrence trends by internal climate variability, the patterns with increasing or decreasing occurrence trends that we identify appear stable throughout the analysis period. Figs. S8–S11 show the occurrence trend analysis for the first or last 20% of circulation pattern occurrences computed using the full reference period. With the exception of circulation patterns with decreasing occurrence trends in winter, which have a very small sample size, there is very little difference between the two timeperiods considered.

## Magnitude of trends per decade

Table S1 shows the magnitude of the trends for days with significant occurrence trends, estimated for each dataset or variable whose analysis is reported in Figs. 1, 2, S4–7, S12–15 and S18–19. The trends are averaged over the different quantiles used for the analyisis and are always expressed in terms of number of analogues/decade. There is a close match between ERA5 and NCEP trends for sea-level pressure and no difference when trends are estimated on ERA5 with a cubic rather than a linear fit. When increasing the number of periods from 9 to 14 (that is from 8 years to 5 years bin lengths), the absolute value of trends slightly reduces. Trends for 500 hPa geopotential height are larger in absolute values. Overall we have that increasing (resp. decreasing) trends induce between 2 and 4 analogues more (resp. less) every decade.

## References


1. Kalnay E, et al. (1996) The ncep/ncar 40-year reanalysis project. *Bulletin of the American meteorological Society* 77(3):437–472.
2. Kornhuber K, et al. (2020) Amplified rossby waves enhance risk of concurrent heatwaves in major breadbasket regions. *Nature Climate Change* 10(1):48–53.
3. Rogers CD, Kornhuber K, Perkins-Kirkpatrick SE, Loikith PC, Singh D (2022) Sixfold increase in historical northern hemisphere concurrent large heatwaves driven by warming and changing atmospheric circulations. *Journal of Climate* 35(3):1063–1078.
4. Huang B, et al. (2017) Extended reconstructed sea surface temperature, version 5 (ersstv5): upgrades, validations, and intercomparisons. *Journal of Climate* 30(20):8179–8205.
5. Barnston AG, Livezey RE (1987) Classification, seasonality and persistence of low-frequency atmospheric circulation patterns. *Monthly weather review* 115(6):1083–1126.
6. L'Heureux ML, Collins DC, Hu ZZ (2013) Linear trends in sea surface temperature of the tropical pacific ocean and implications for the el niño-southern oscillation. *Climate Dynamics* 40(5):1223–1236.
7. L'Heureux ML, Lee S, Lyon B (2013) Recent multidecadal strengthening of the walker circulation across the tropical pacific. *Nature Climate Change* 3(6):571–576.
8. Mezzina B, García-Serrano J, Bladé I, Kucharski F (2020) Dynamics of the enso teleconnection and nao variability in the north atlantic–european late winter. *Journal of Climate* 33(3):907–923.
9. Paciorek CJ, Stone DA, Wehner MF (2018) Quantifying statistical uncertainty in the attribution of human influence on severe weather. *Weather and climate extremes* 20:69–80.

| Dataset-Variable (N periods) [Type of fit] | Winter | | Summer | |
|---|---|---|---|---|
| | Increasing | Decreasing | Increasing | Decreasing |
| ERA5-SLP (9) [linear] | 3.7±1.0 | -3.1±0.7 | 3.6±0.9 | -2.9±0.5 |
| ERA5-SLP (14) [linear] | 2.3±0.5 | -2.2±0.4 | 2.4±0.5 | -2.0±0.3 |
| ERA5-SLP (9) [cubic] | 3.7±1.0 | -3.1±0.7 | 3.6±0.9 | -2.9±0.5 |
| ERA5-Z500 (9 ) [linear] | 4.1±1.1 | -4.1±1.1 | 4.2±1.2 | -3.2±0.8 |
| NCEP-SLP (9) [linear] | 3.9±1.0 | -3.2±0.7 | 4.0 ±1.1 | -4.3±1.2 |

**Table S1. Magnitude of trends estimated for different datasets, variables and number of periods for which the trends are computed over the 73 years of data. 9 periods correspond to roughly 8 years bin lengths, 14 periods to roughly 5 years bin lengths. The type of fit indicates whether a linear or a cubic fit has been applied to the data. The magnitude of all trends is expressed in Number of analoges/decade, so that results are comparable. Trends are averaged over the three different quantiles used in the study: $q = 0.98$, $0.99$ and $0.995$, and for all the days displaying increasing or decreasing occurrence trends in Winter or in Summer. The uncertainty is given in terms of one standard deviation of the mean.**

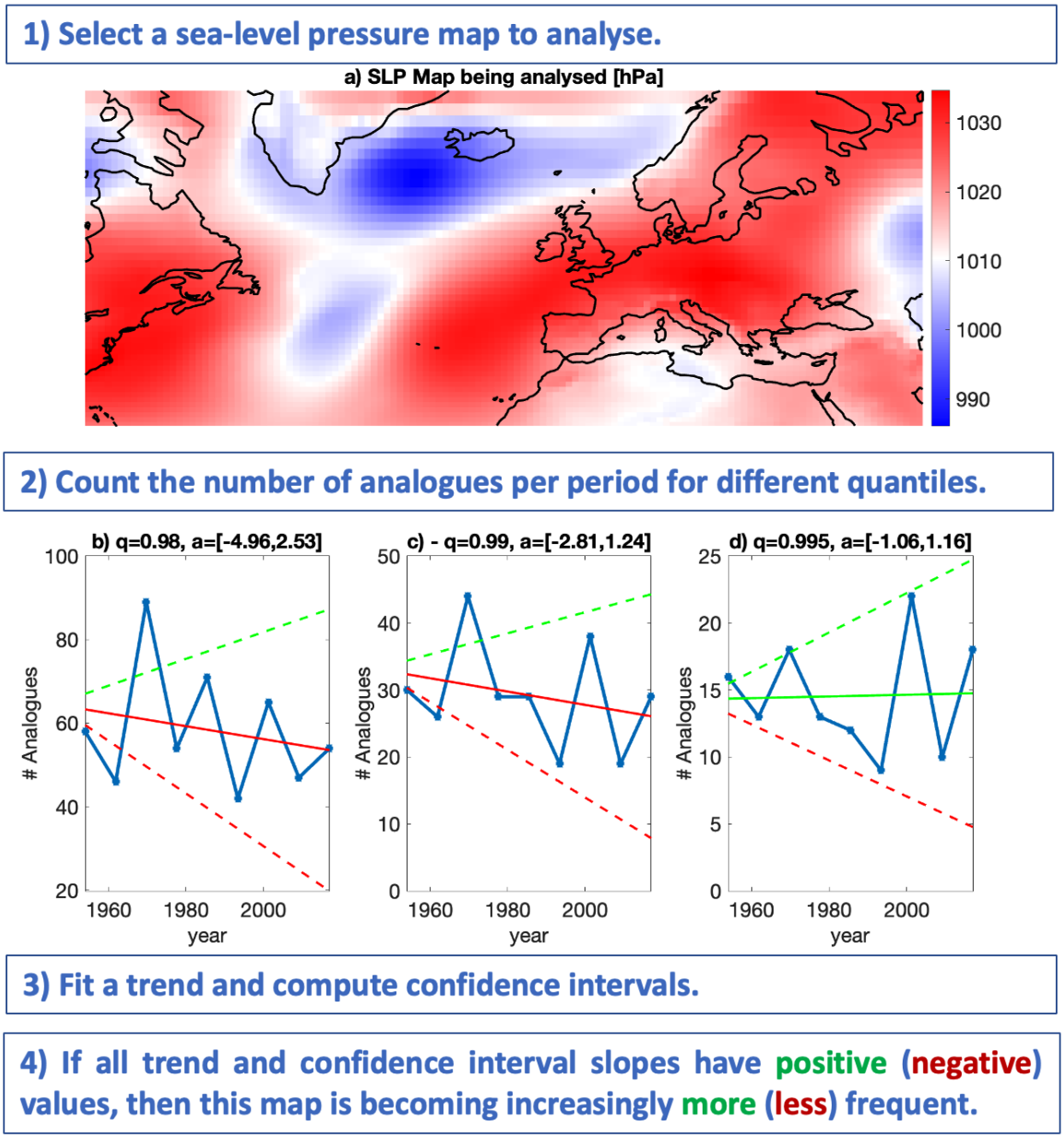


**Fig. S1. Example of the procedure applied in the manuscript to detect daily sea-level pressure maps with increasing or decreasing occurrence trend:** The sea-level pressure map for 01/01/1950 is shown in panel (a). The best 2% (b), 1% (c) and 0.5% (d) of analogues are searched in a database consisting of n=26280 daily sea-level pressure maps from ERA5 starting in January 1950. These correspond to the quantiles $q = 0.98, 0.99$ and $0.995$, respectively. The number of analogues (# Analogues) counted in each period of 7.5 years are then obtained (blue dots, panels b–d). A linear fit is performed and the confidence intervals for the slope $a$ are computed (dotted lines and values in square brackets). Lines with positive (negative) slopes are coloured green (red). A daily sea-level pressure map displays a significant trend if all lines in panels (b—d) display the same color (red or green). This is not the case for the map 01/01/1950, taken in this example.

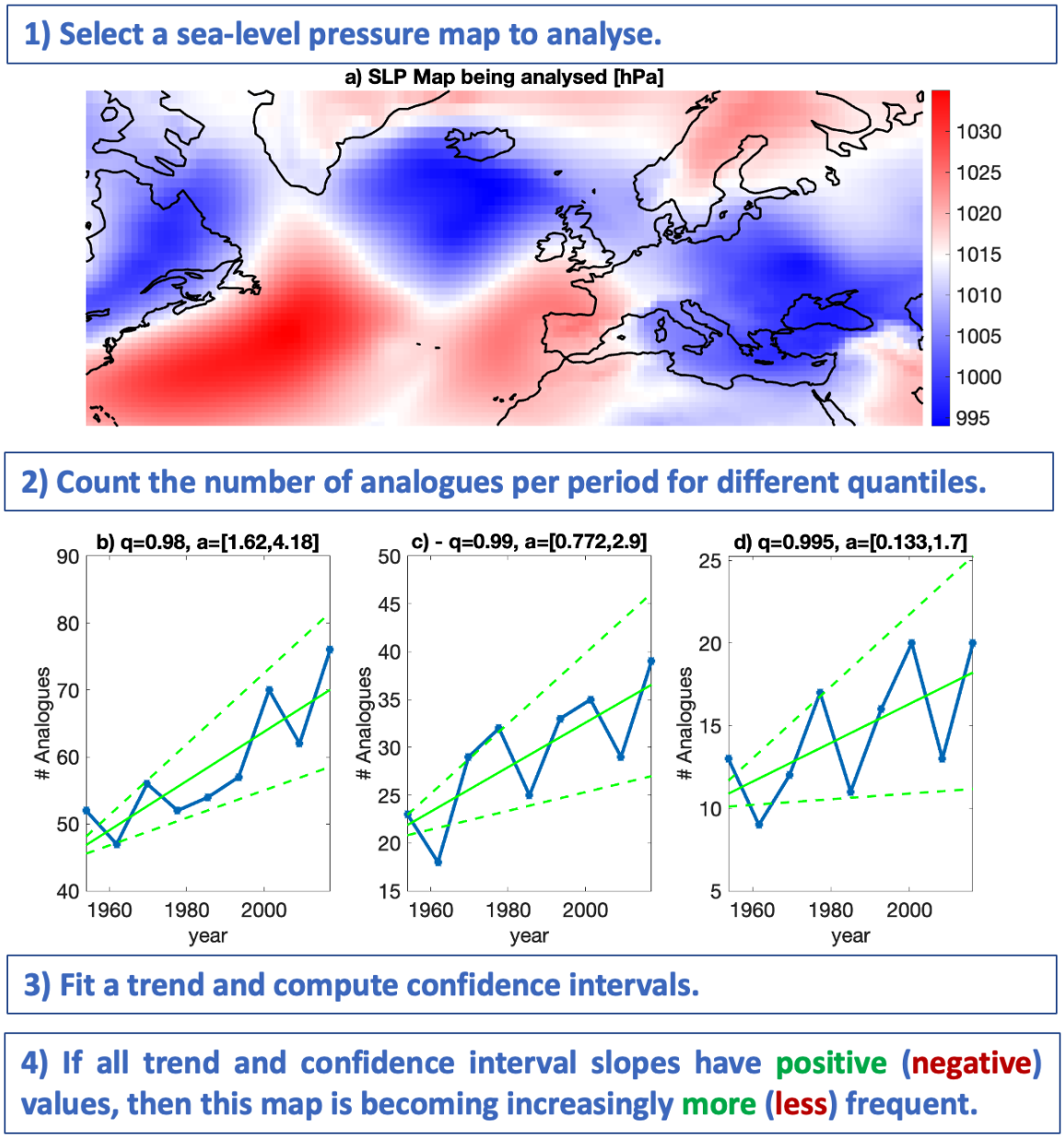


**Fig. S2. Example of the procedure applied in the manuscript to detect daily sea-level pressure maps with increasing or decreasing occurrence trend:** As Fig. S1, but for 04/01/1950 which does display a significant positive occurrence trend.

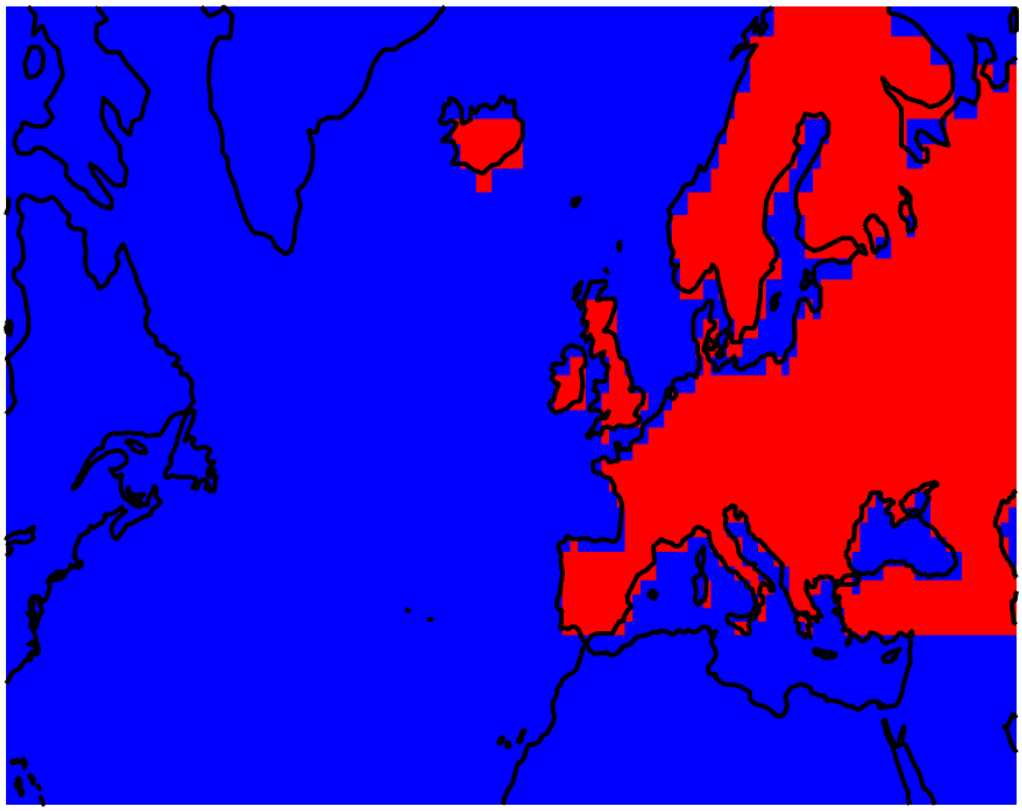

**Fig. S3. European mask used to compute timeseries of continental European data:** Red shading shows the gridboxes used to compute timeseries of continental European data shown in panels i, j of Figs. 1, 2 and S4–S19.

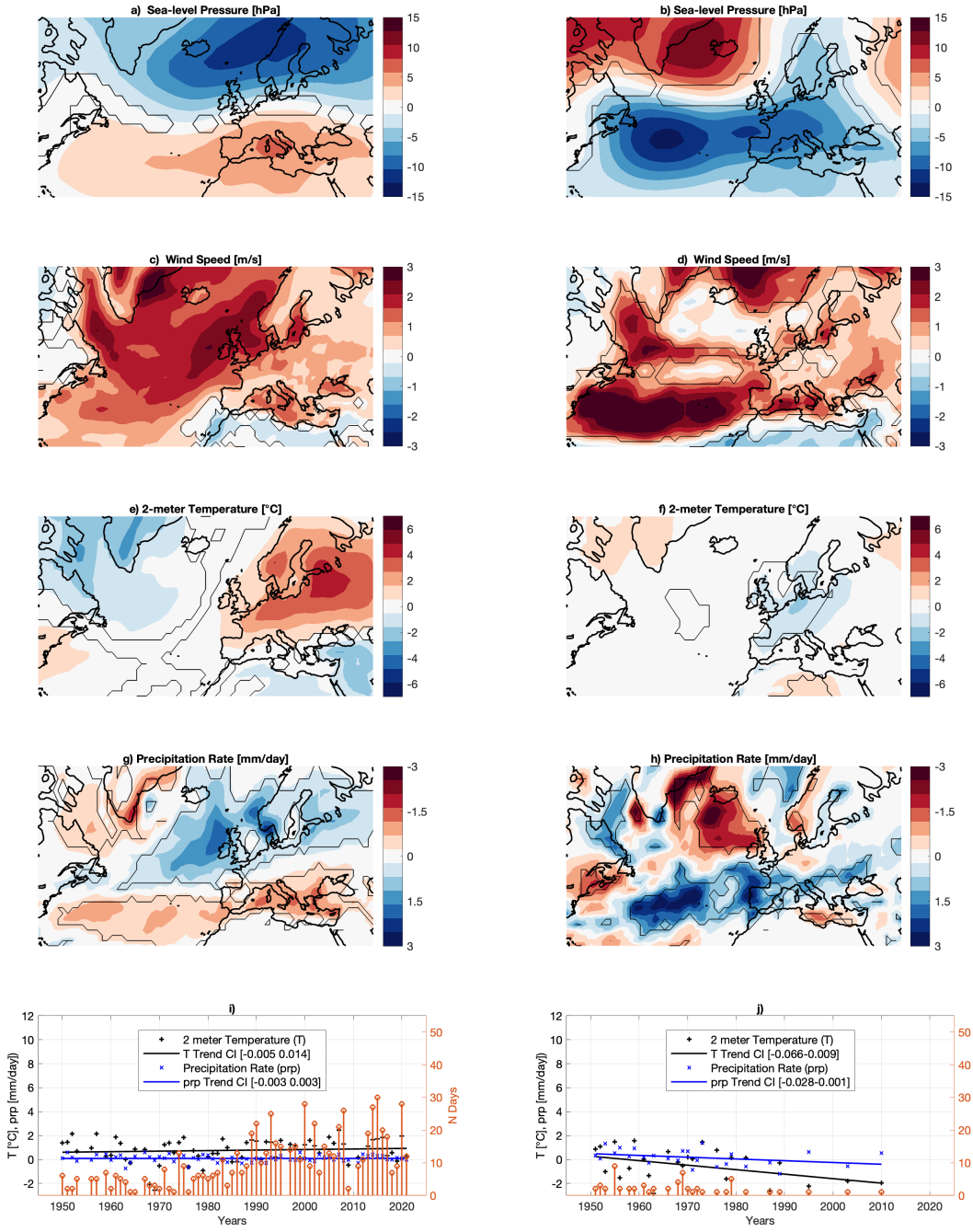


**Fig. S4. Sea-level pressure wintertime atmospheric circulation patterns with significant occurrence trends and associated surface anomalies:** As in Fig. 1, but for NCEP-NCAR reanalysis data.

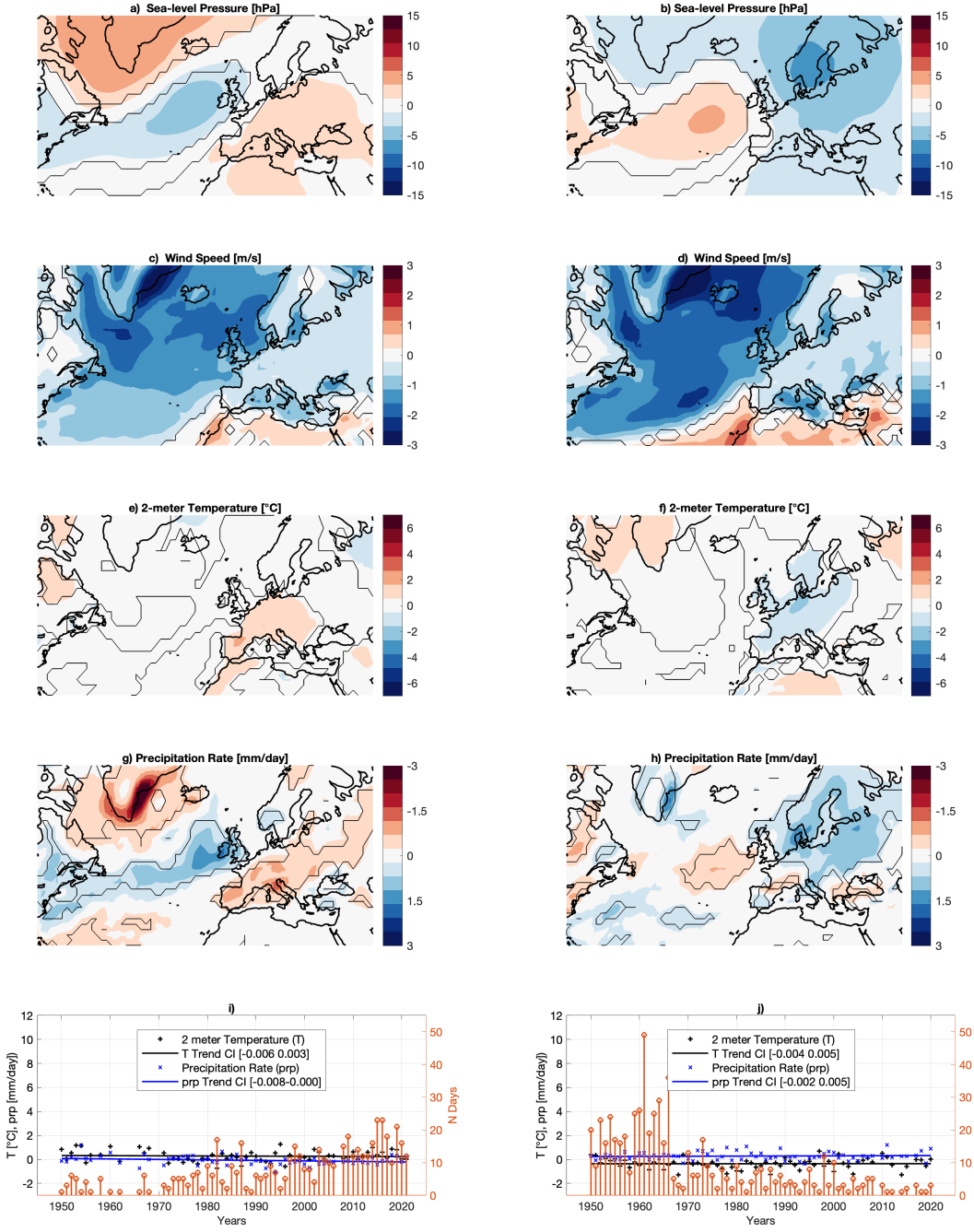


**Fig. S5. Sea-level pressure summertime atmospheric circulation patterns with significant occurrence trends and associated surface anomalies:** As in Fig. 2, but for NCEP-NCAR reanalysis data.

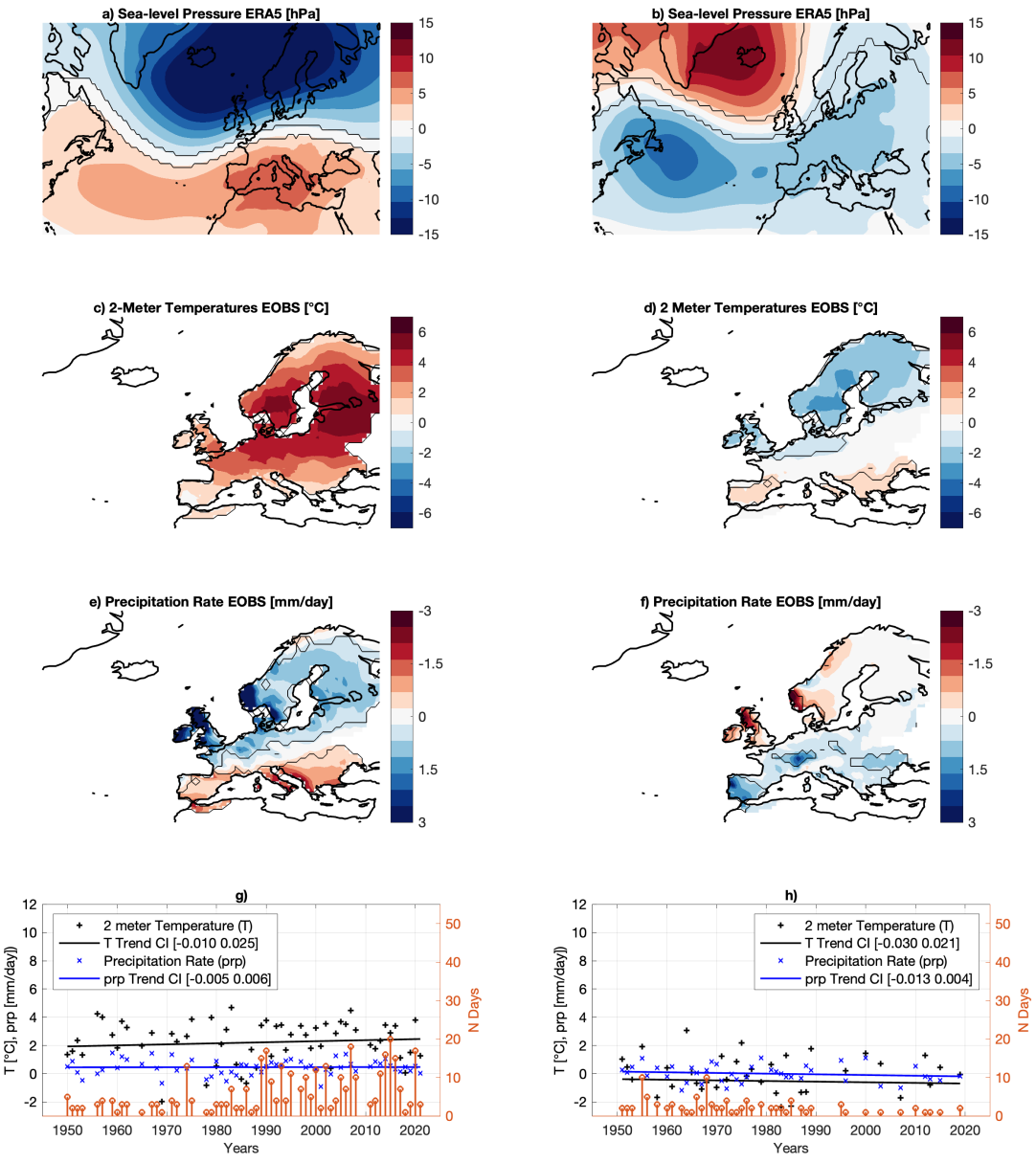


**Fig. S6. Sea-level pressure wintertime atmospheric circulation patterns with significant occurrence trends and associated surface anomalies:** As in Fig. 1, but for ERA5 sea-level pressure data (a, b) and E-OBS temperature and precipitation (c–f). The figure does not include wind data.

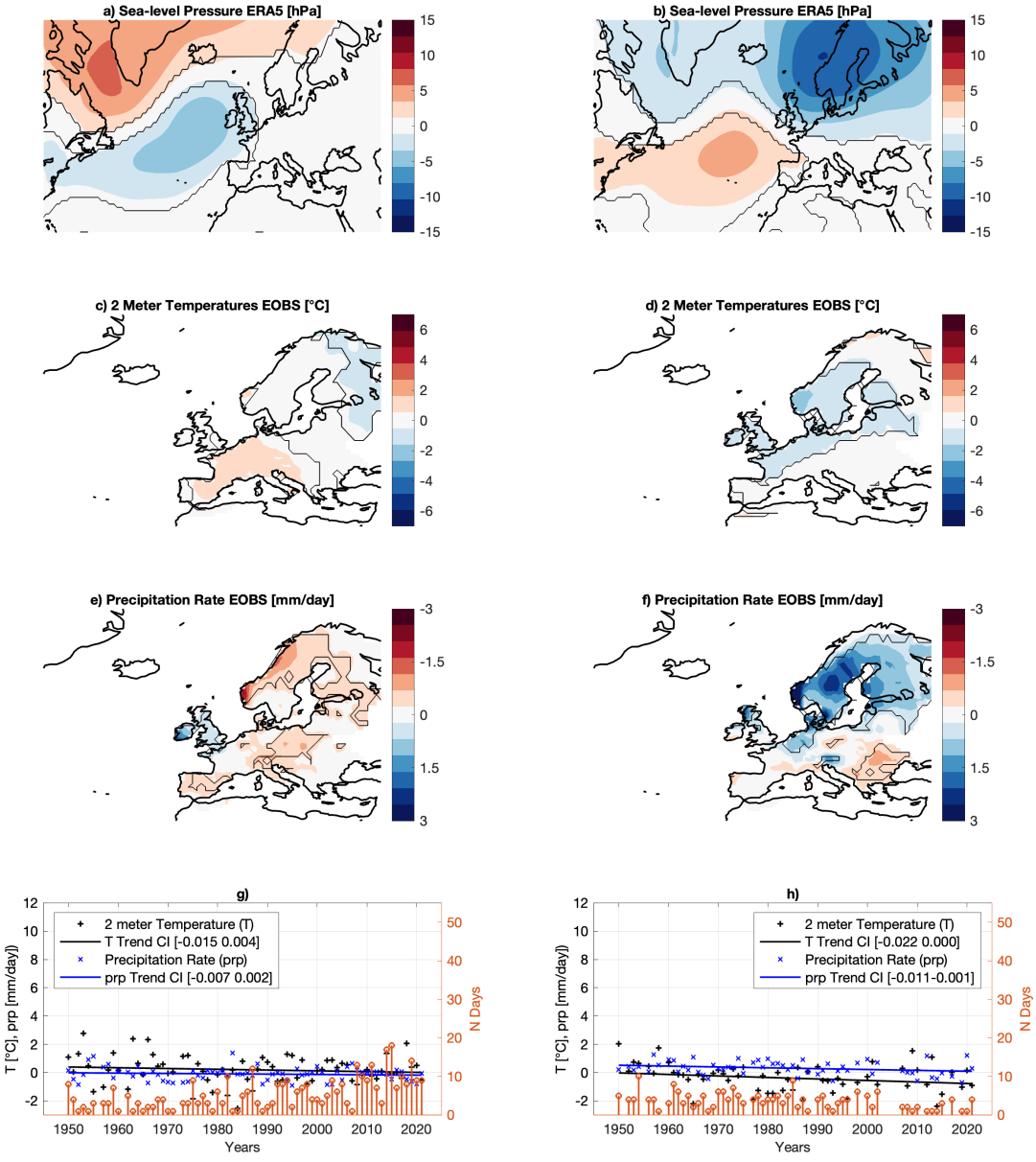


**Fig. S7. Sea-level pressure summertime atmospheric circulation patterns with significant occurrence trends and associated surface anomalies:** As in Fig. 2, but for ERA5 sea-level pressure data data (a, b) and E-OBS 2-metre temperature and precipitation (c–f). The figure does not include wind data.

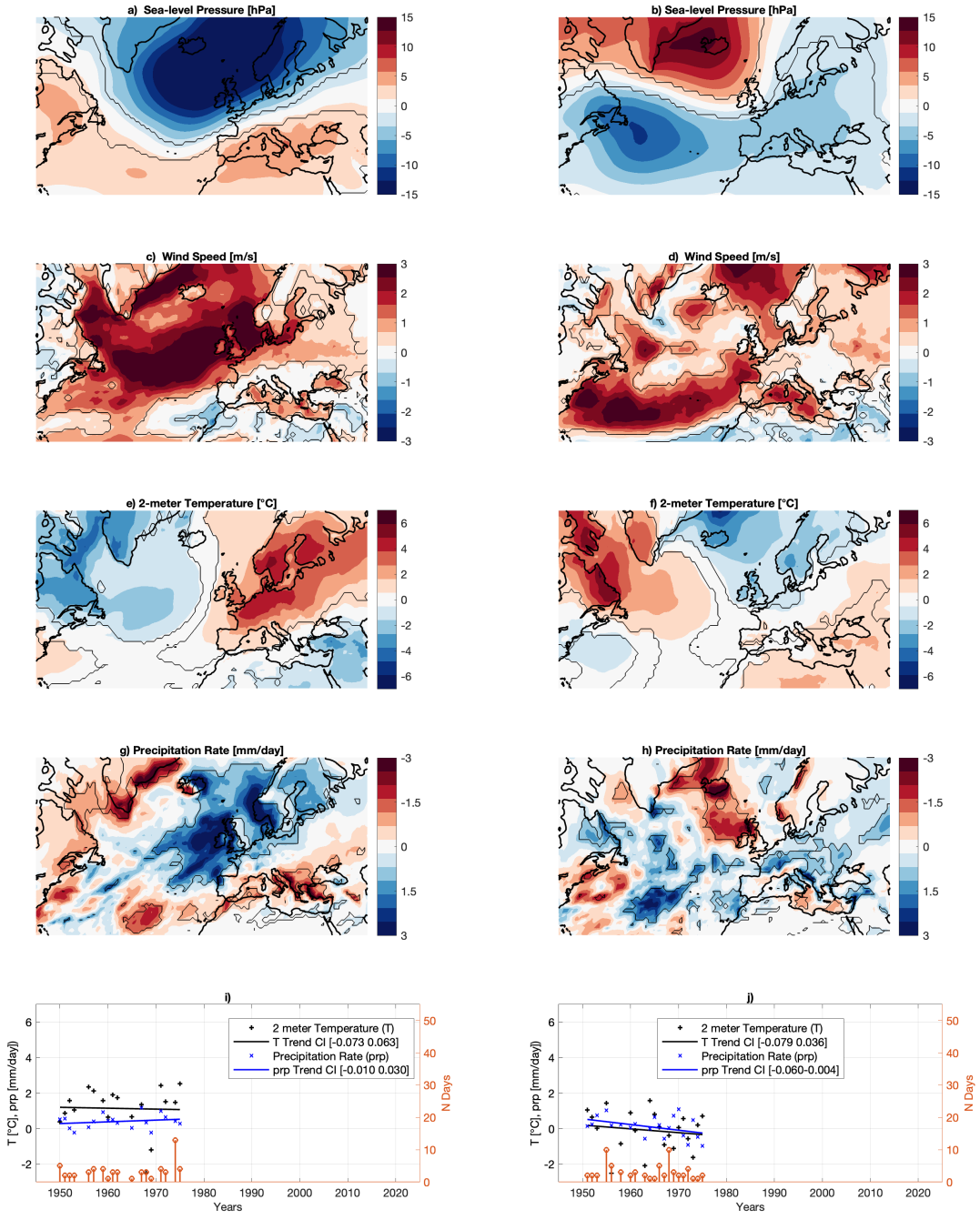


**Fig. S8. First 25 years of the sea-level pressure wintertime atmospheric circulation patterns with significant occurrence trends and associated surface anomalies:** As in Fig. 1, but for the earliest 25 years in the dataset.

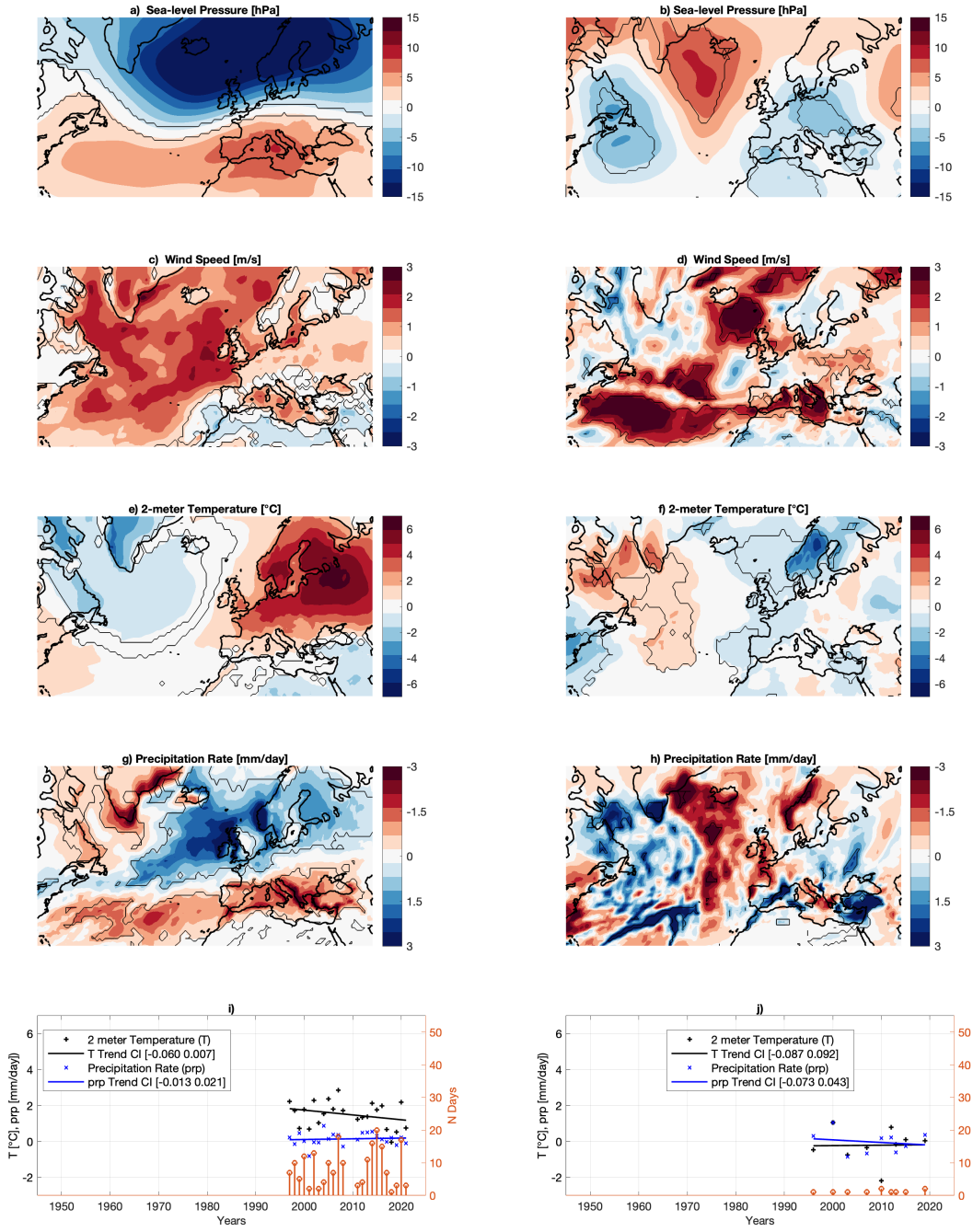


**Fig. S9. Last 25 years of the sea-level pressure wintertime atmospheric circulation patterns with significant occurrence trends and associated surface anomalies:** As in Fig. 1, but for the latest 25 years in the dataset.

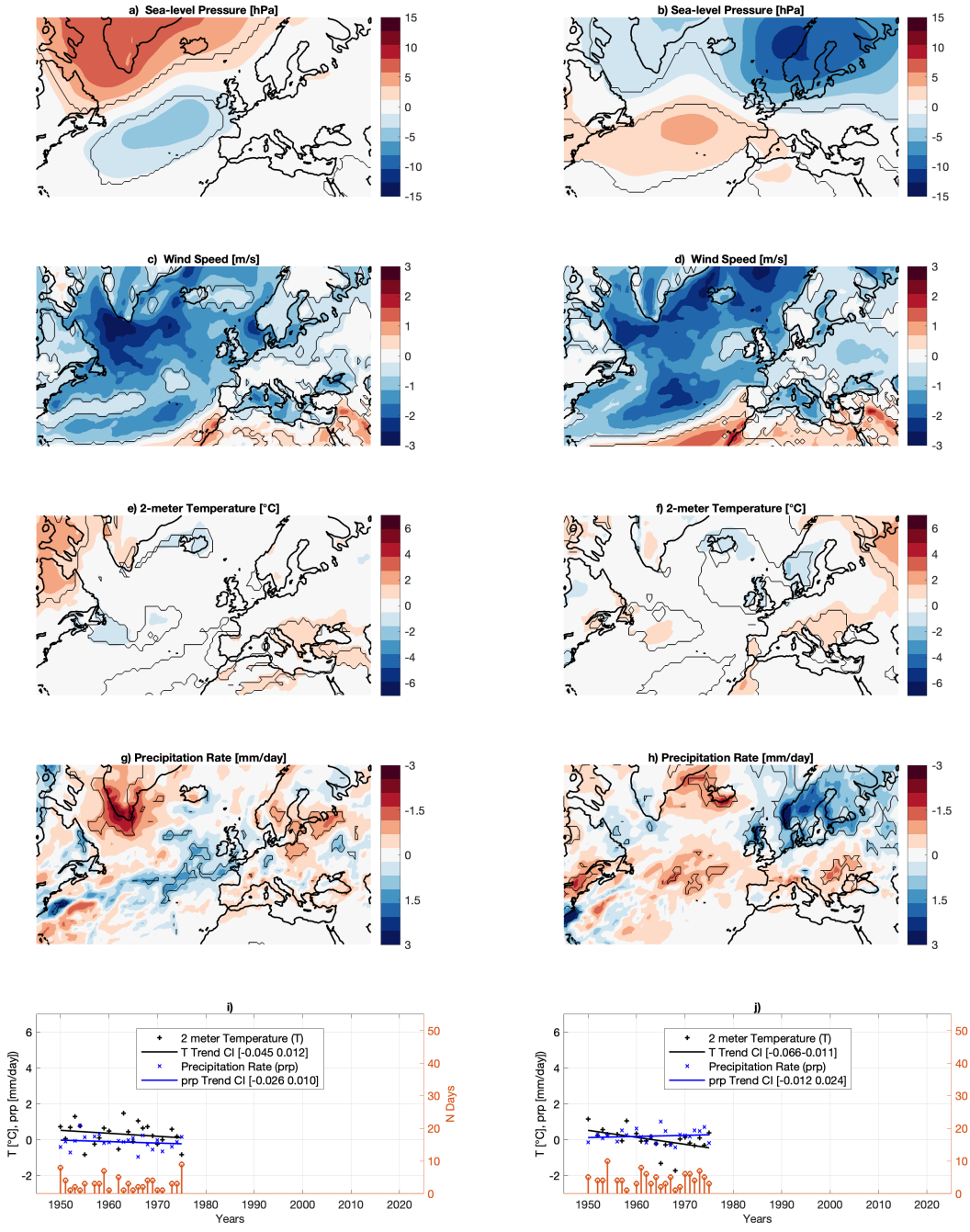


**Fig. S10. First 25 years of the sea-level pressure summertime atmospheric circulation patterns with significant occurrence trends and associated surface anomalies:** As in Fig. 2, but for the earliest 25 years in the dataset.

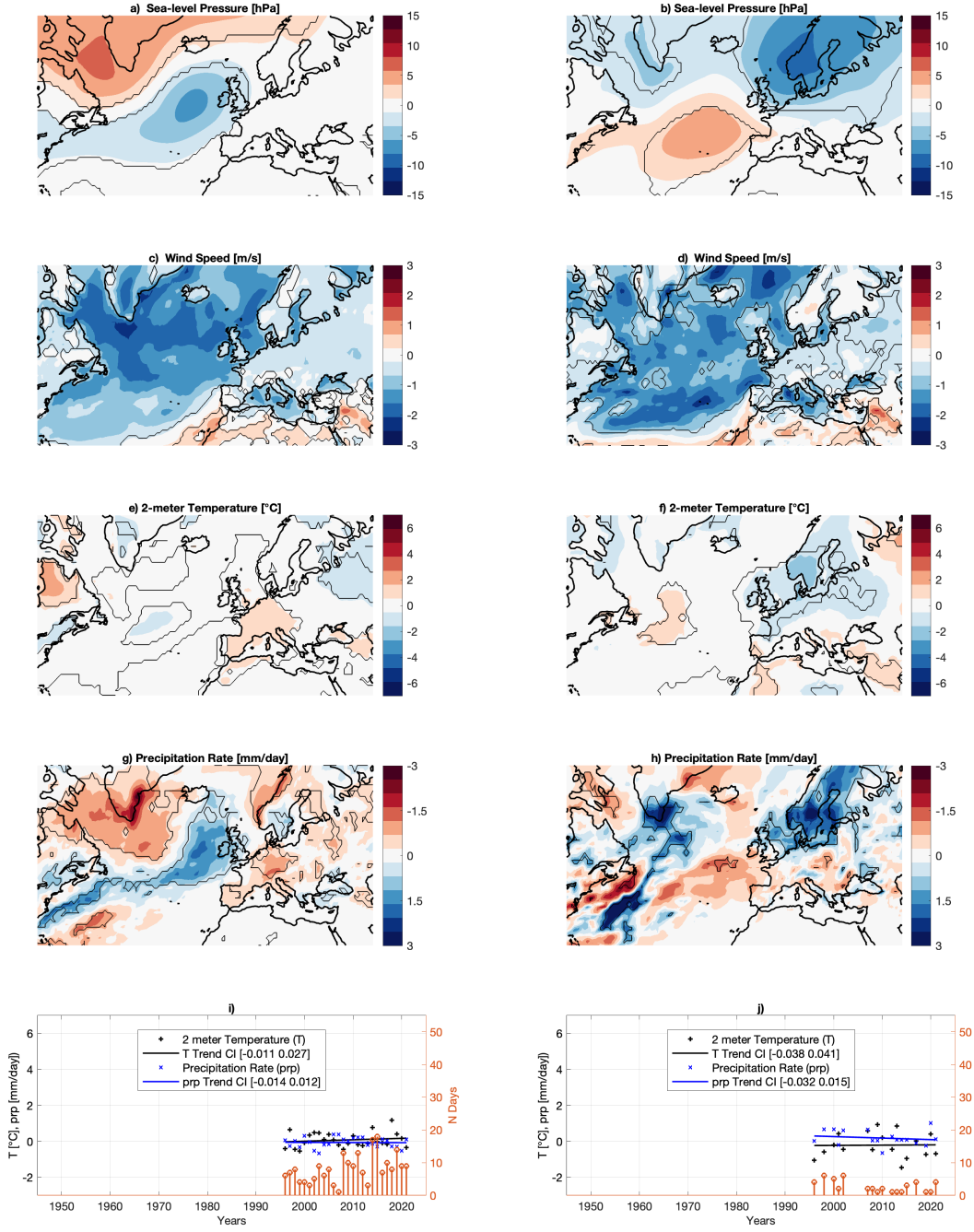


**Fig. S11. Last 25 years of the sea-level pressure summertime atmospheric circulation patterns with significant occurrence trends and associated surface anomalies:** As in Fig. 2, but for the latest 25 years in the dataset.

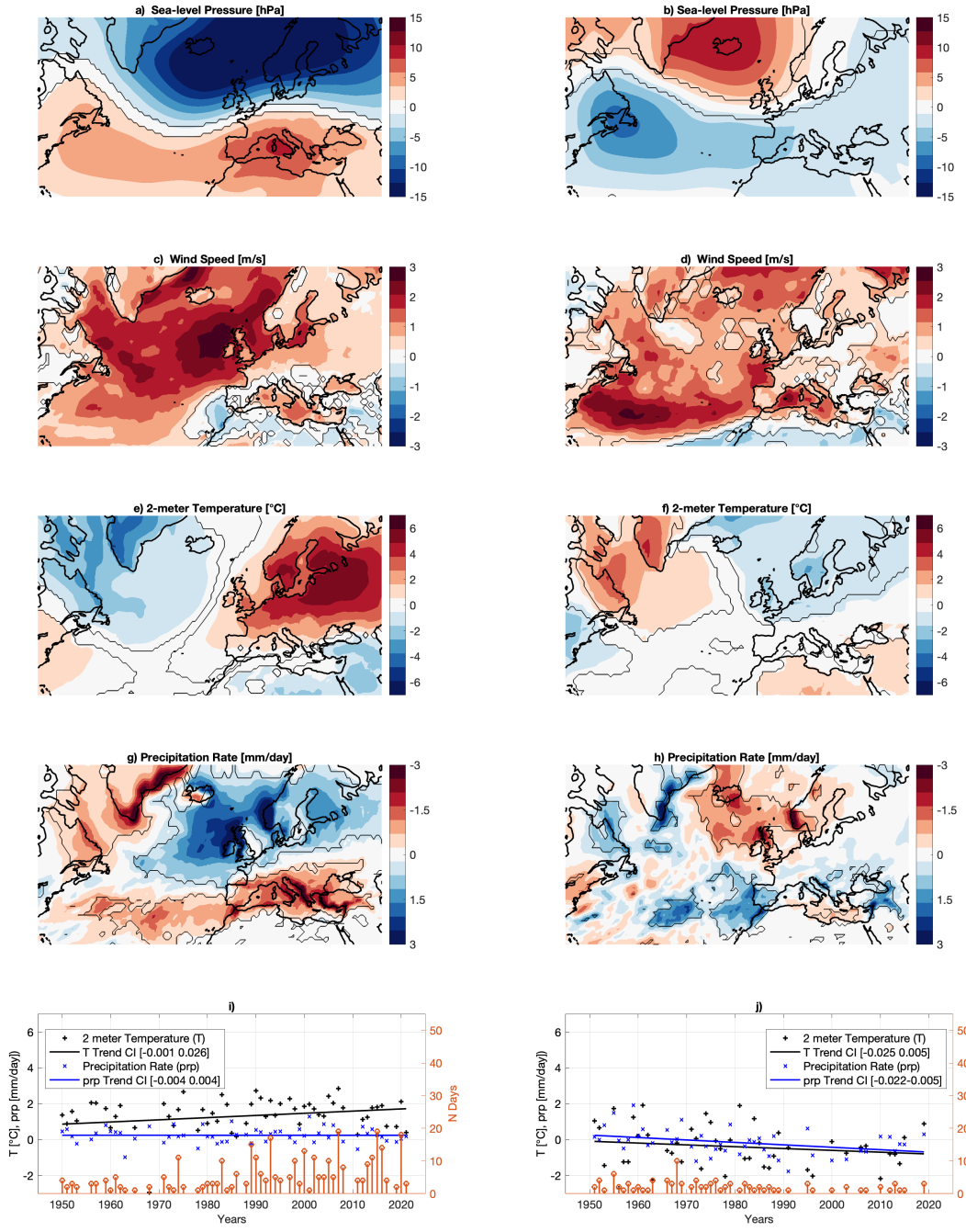


**Fig. S12. Sea-level pressure wintertime atmospheric circulation patterns with significant occurrence trends and associated surface anomalies:** As in Fig. 1, but dividing the time interval of 73 years in 14 periods of roughly 5 years.

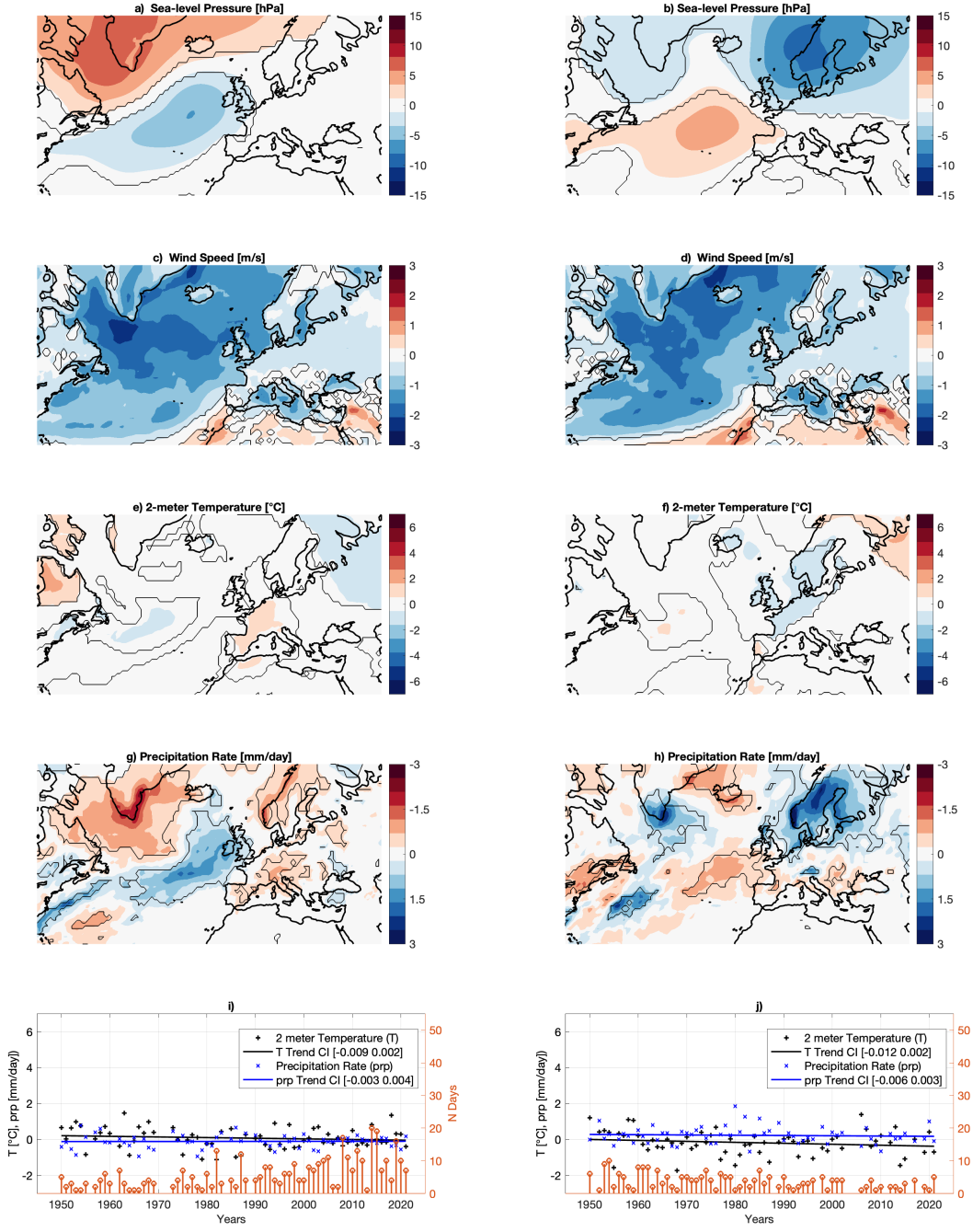


**Fig. S13. Sea-level pressure wintertime atmospheric circulation patterns with significant occurrence trends and associated surface anomalies:** As in Fig. 2, but dividing the time interval of 73 years in 14 periods of roughly 5 years.

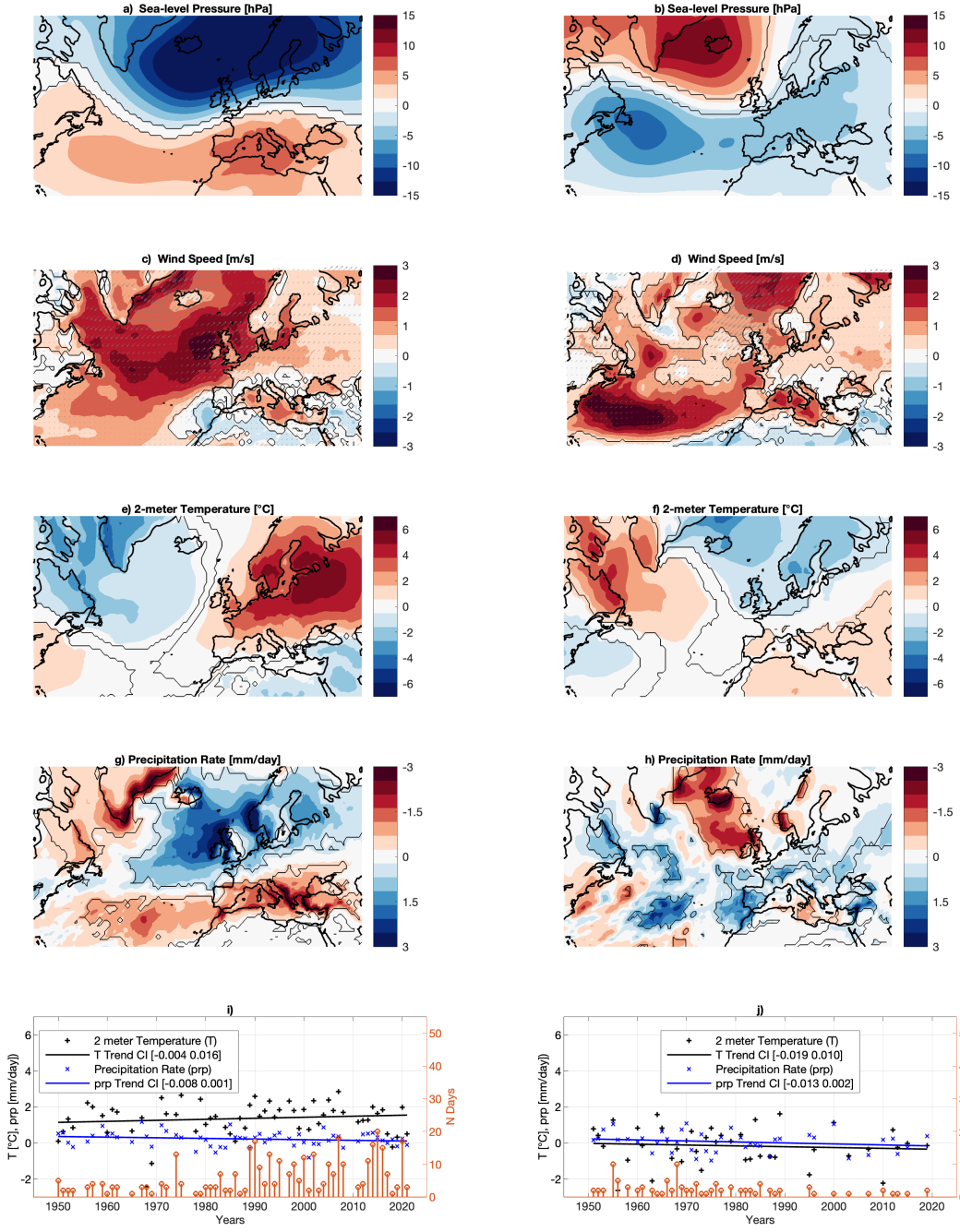


**Fig. S14. Sea-level pressure wintertime atmospheric circulation patterns with significant occurrence trends and associated surface anomalies:** As in Fig. 1, but when applying cubic fits (instead of linear) to the data.

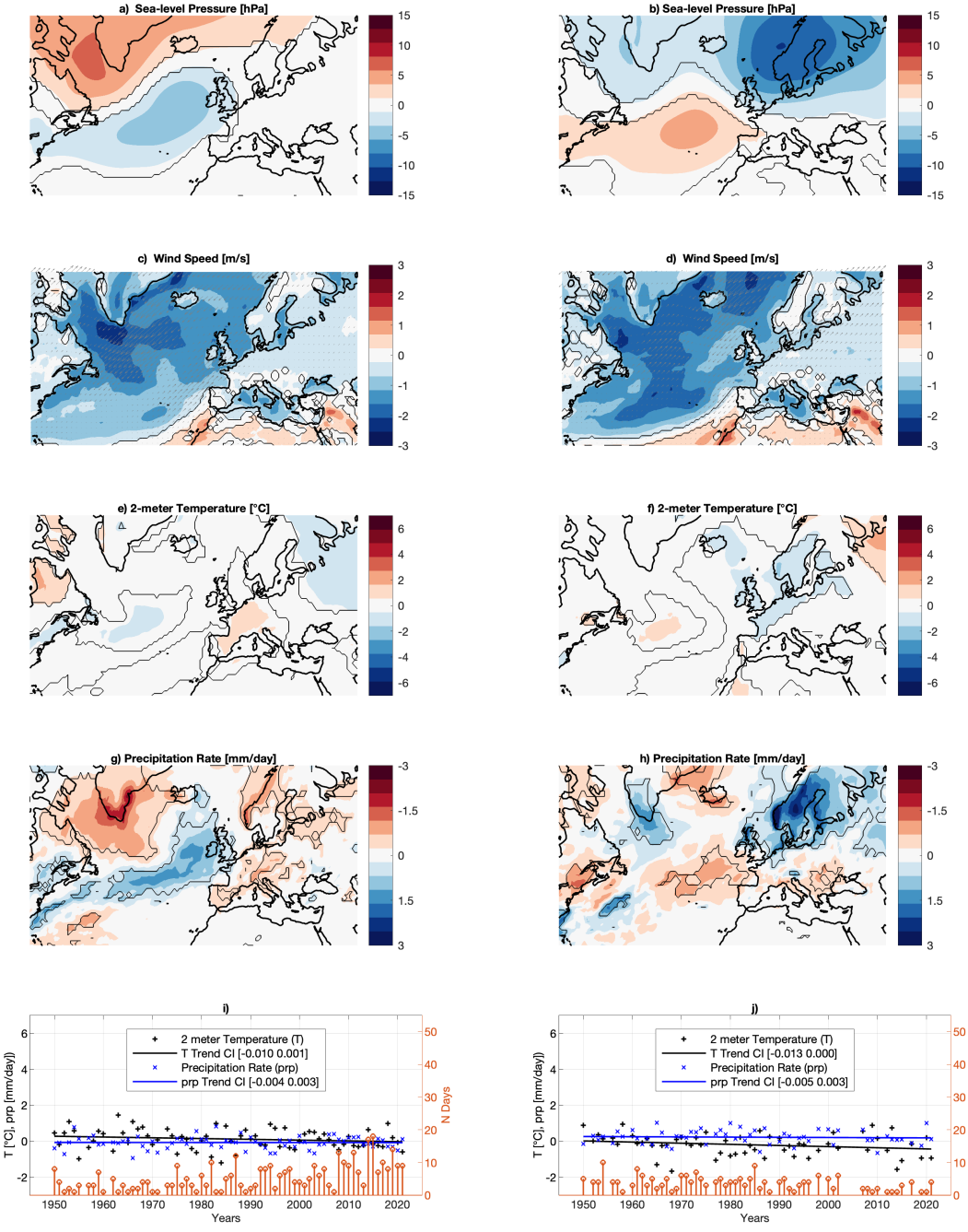


**Fig. S15. Sea-level pressure wintertime atmospheric circulation patterns with significant occurrence trends and associated surface anomalies:** As in Fig. 2, but when applying cubic fits (instead of linear) to the data.

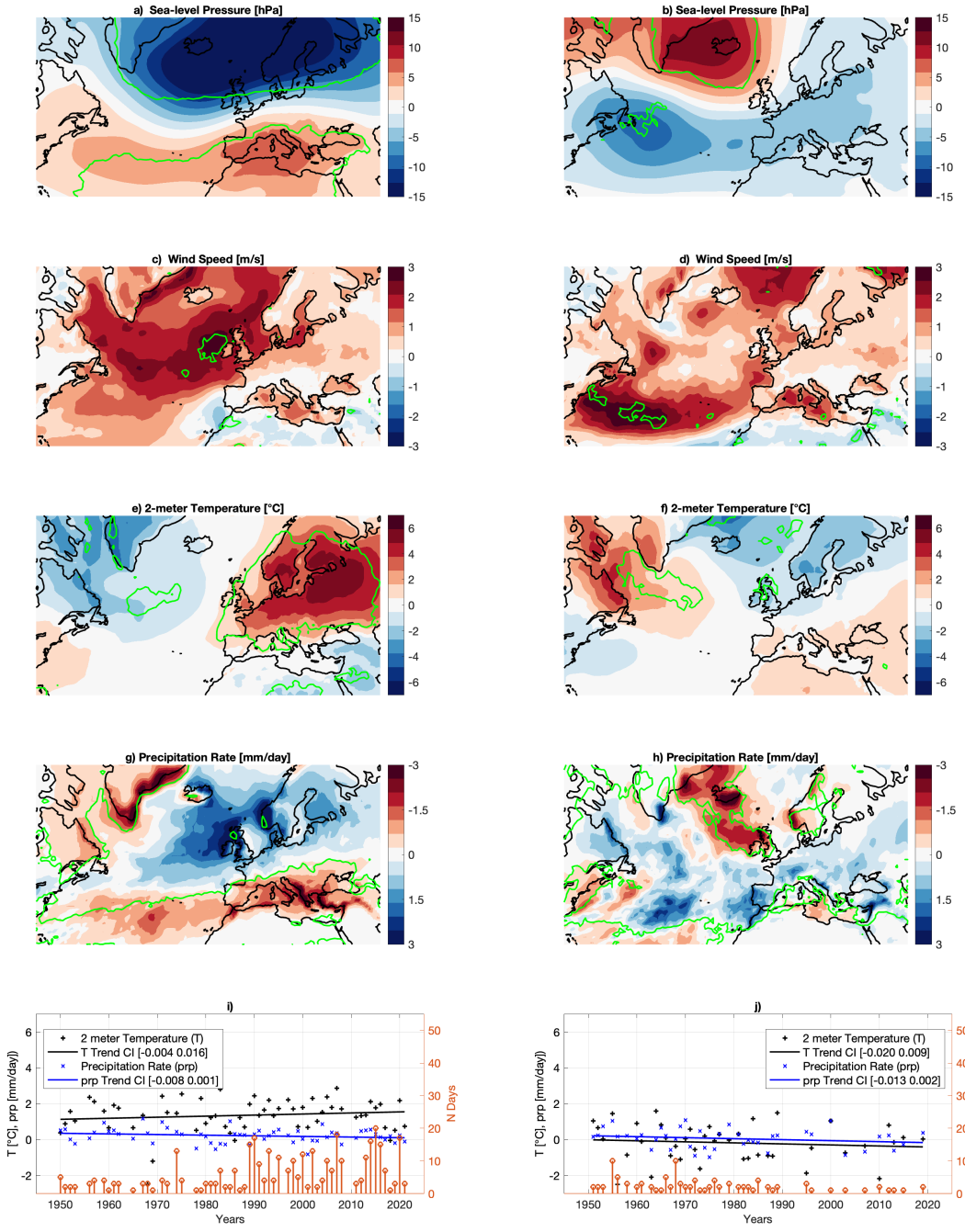


**Fig. S16. Sea-level pressure wintertime atmospheric circulation patterns with significant occurrence trends and associated surface anomalies:** As in Fig. 1, but where green contours indicate regions where 75% of the days display anomalies of the same sign.

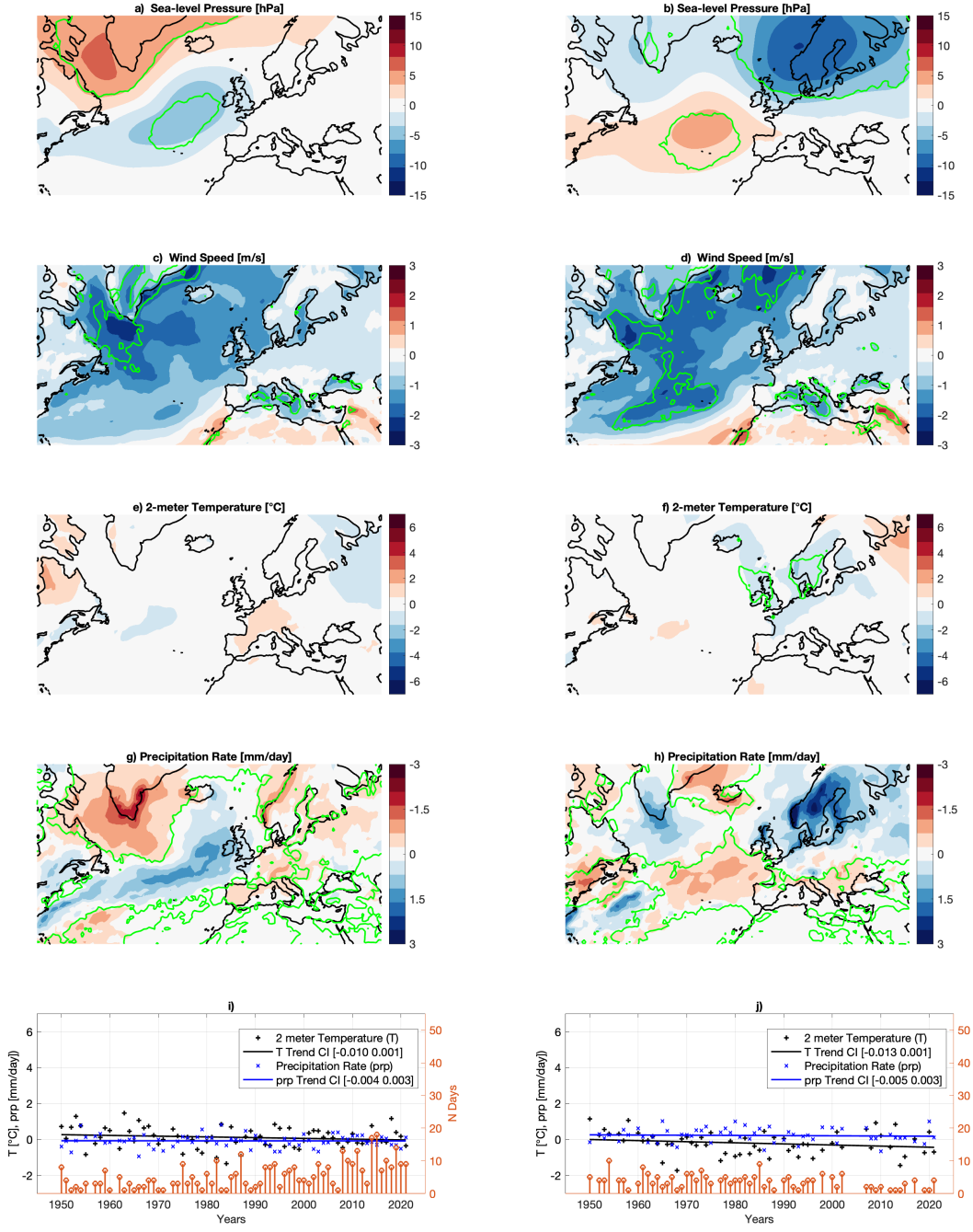


**Fig. S17. Sea-level pressure wintertime atmospheric circulation patterns with significant occurrence trends and associated surface anomalies:** As in Fig. 2,but where green contours indicate regions where 75% of the days display anomalies of the same sign.

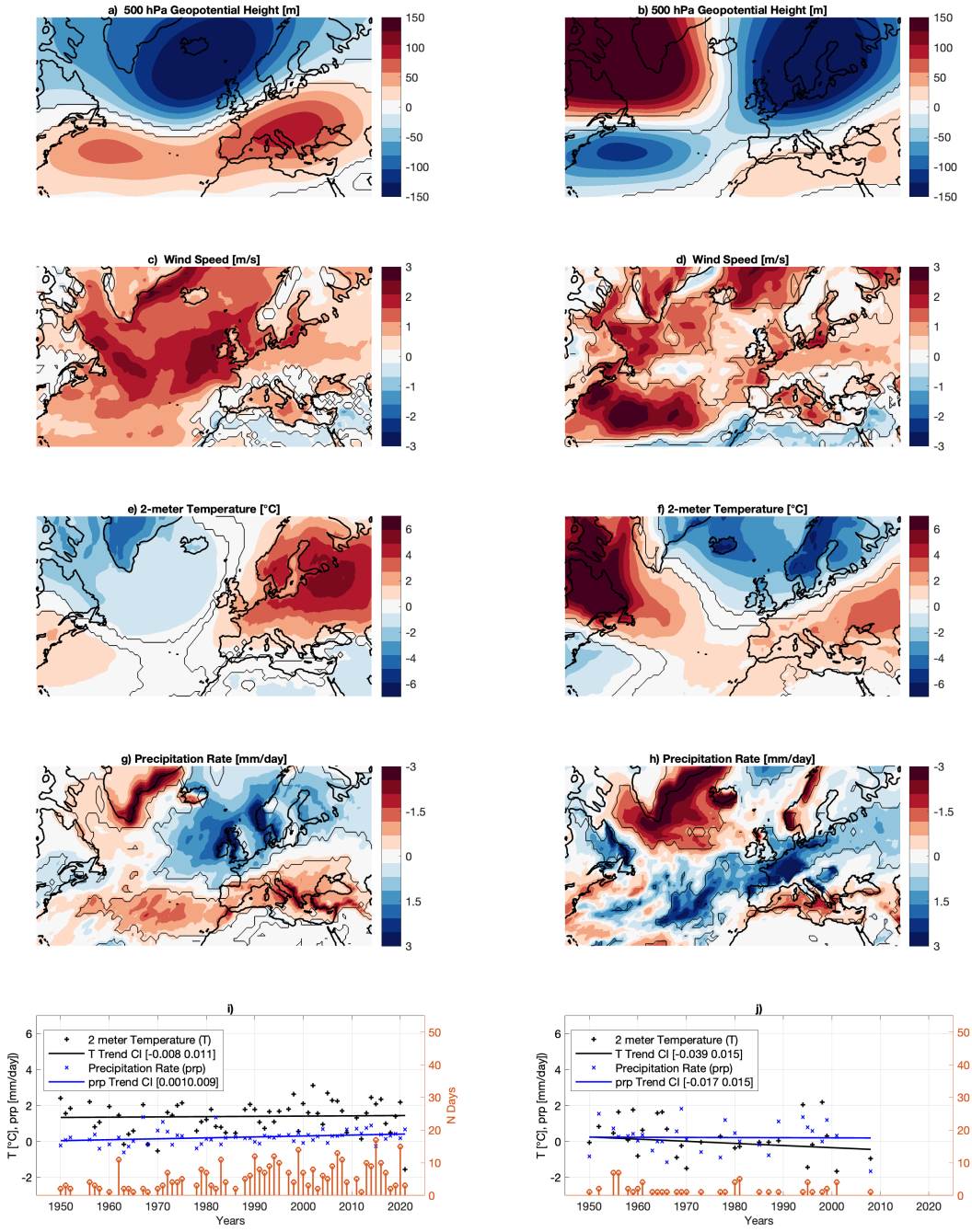


**Fig. S18. 500 hPa geopotential height wintertime atmospheric circulation patterns with significant occurrence trends and associated surface anomalies:** As in Fig. 1, but for 500 hPa geopotential height data from ERA5 (a,b).

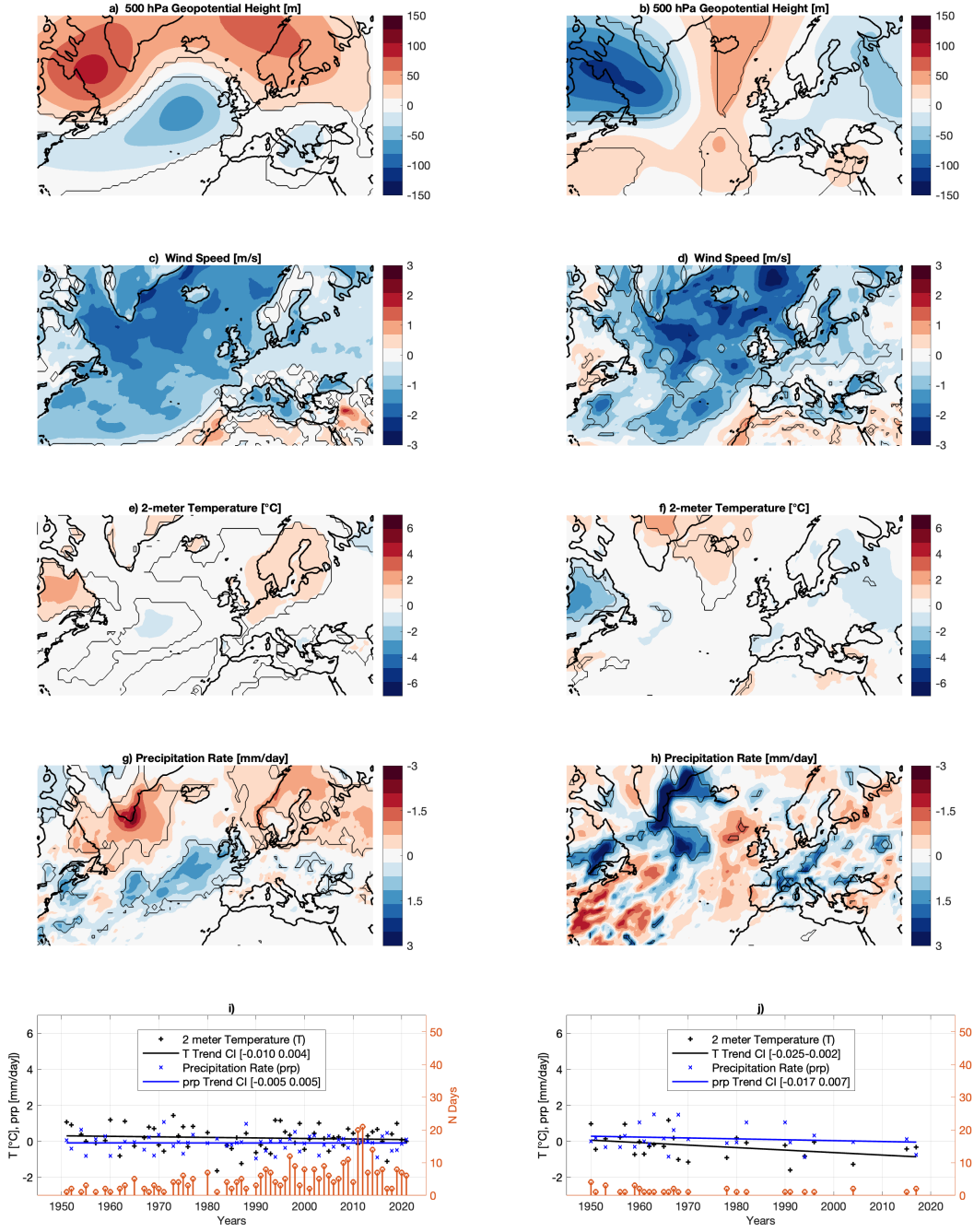


**Fig. S19. 500 hPa geopotential height summertime atmospheric circulation patterns with significant occurrence trends and associated surface anomalies:** As in Fig. 2, but for 500 hPa geopotential height data from ERA5 (a,b).

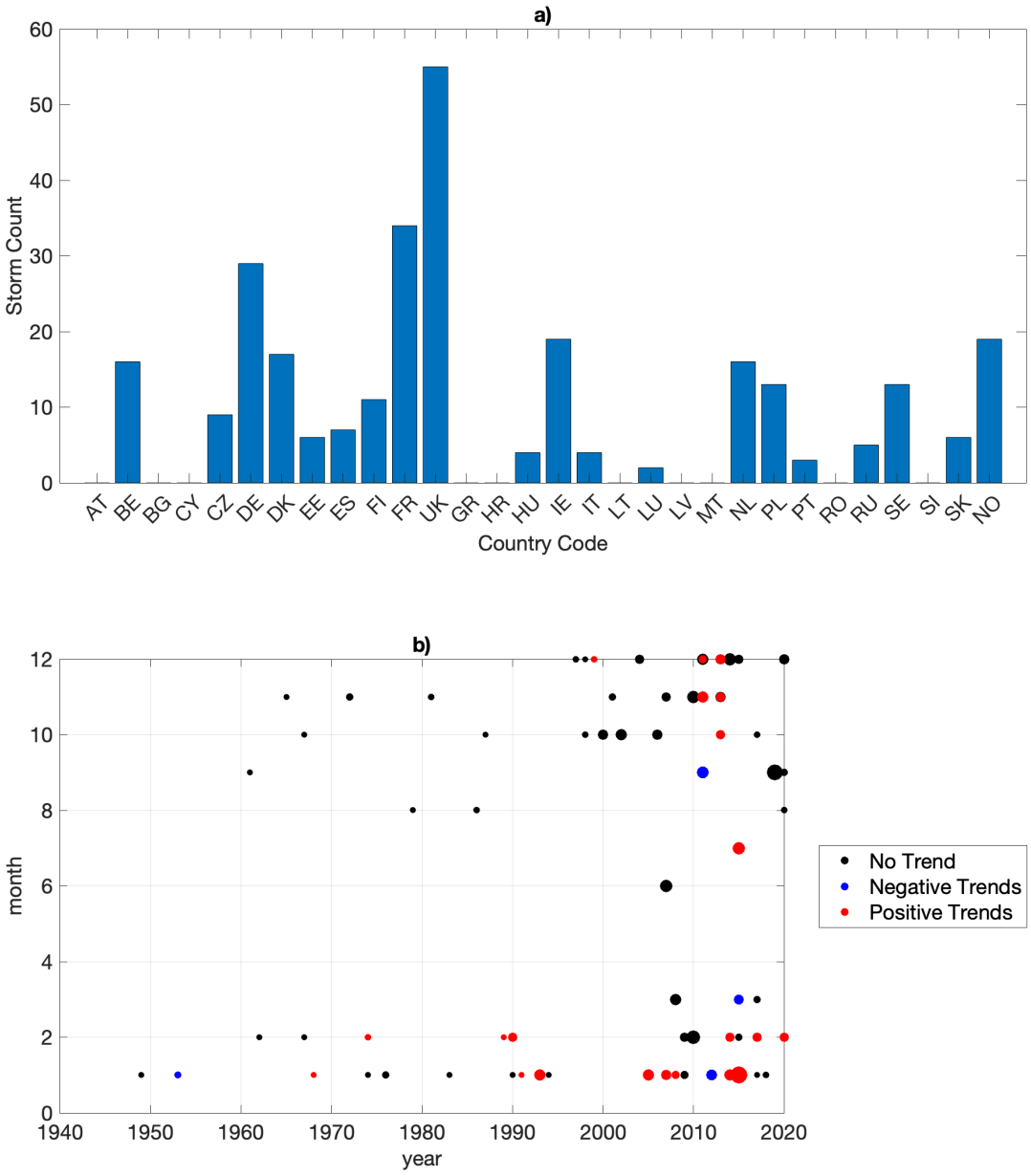


**Fig. S20. Spatial and temporal distribution of European windstorms**: Number of European Windstorms per country (a). Year and month of occurrence of each storm and duration (size of the balls). Colours show storms associated with atmospheric patterns displaying no (black), negative (blue) or positive (red) occurrence trends (b).

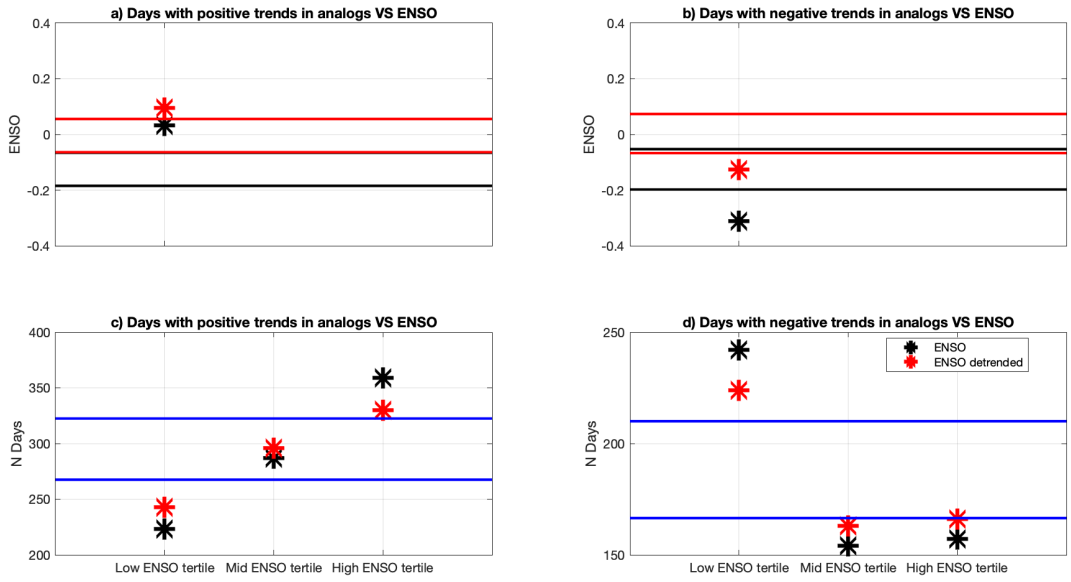


**Fig. S21. Monthly El Nino – Southern Oscillation values conditioned on days with significant occurrence trends and count of days with significant occurrence trends corresponding to different El Nino – Southern Oscillation phases:** Averages of monthly ENSO 3.4 values conditioned on positive (a) or negative (b) occurrence trends (stars). Number of days with positive (c) or negative (d) occurrence trends during months with ENSO 3.4 values in the upper (right), middle (center) and lower (left) tertiles of the ENSO 3.4 index distribution. Results for both the raw (black) and the linearly detrended (red) ENSO timeseries are shown. The continuous lines correspond to the 5% significance bounds obtained by a bootstrapping procedure with 500 iterations.

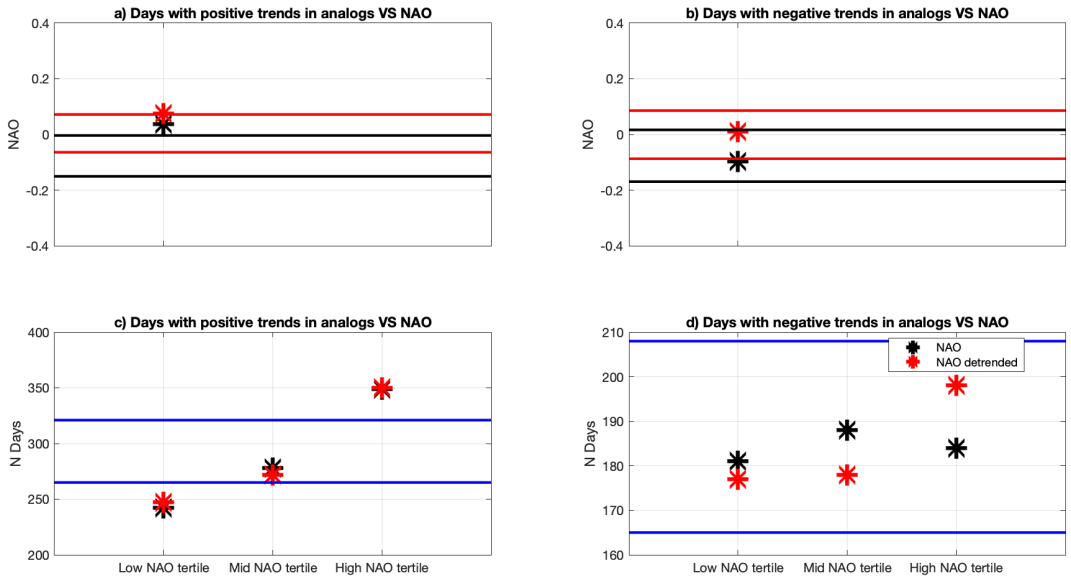


**Fig. S22. Monthly North Atlantic Oscillation values conditioned on days with significant occurrence trends and count of days with significant occurrence trends corresponding to different North Atlantic Oscillation phases:** As in Figure S21 but for the North Atantic Oscillation Index.

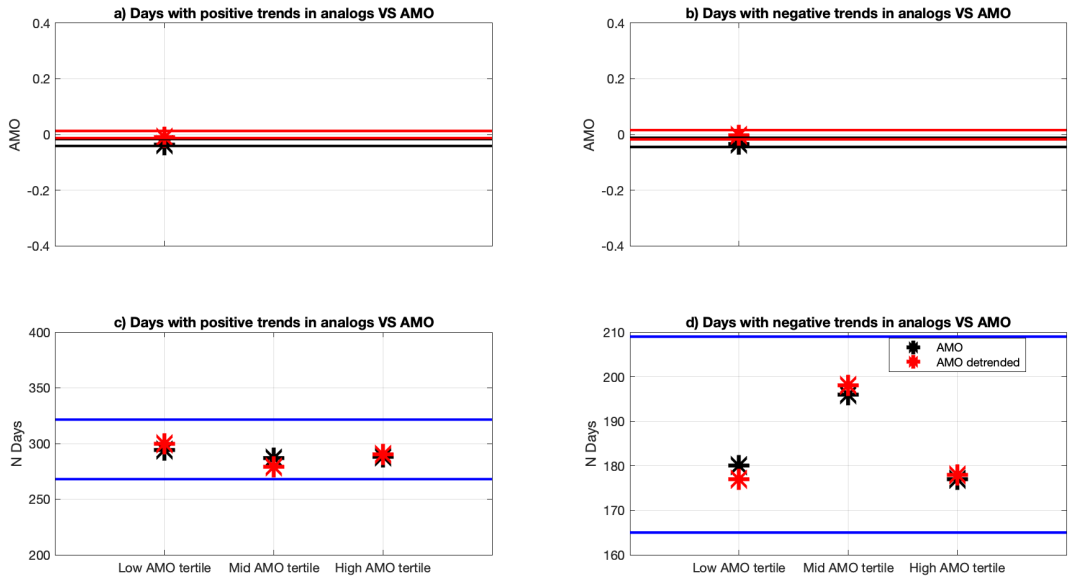


**Fig. S23. Monthly Atlatantic Multidecadal Oscillation values conditioned on days with significant occurrence trends and count of days with significant occurrence trends corresponding to different Atlantic Multidecadal Oscillation phases:** As in Figure S21 but for the Atlantic Multidecadal Oscillation index.